New homochiral and heterochiral Mo(VI) complex from racemic ligand: Synthesis, X-ray structure, diastereomers separation and biological activities

Zahra Kazemi, Hadi Amiri Rudbari, Mehdi Sahihi, Valiollah Mirkhani, Majid Moghadam, Shahram Tangestaninejad, Iraj Mohammadpoor-Baltork, Abolghasem Abbasi Kajani

New homochiral and heterochiral Mo(VI) complex from racemic ligand: Synthesis, X-ray structure, diastereomers separation and biological activities

Author links open overlay panelZahra Kazemi [a], Hadi Amiri Rudbari [a], Mehdi Sahihi [b], Valiollah Mirkhani [a], Majid Moghadam [a], Shahram Tangestani nejad [a], Iraj Mohammadpoor-Baltork [a], Abolghasem Abbasi Kajani [a]

[a] Department of Chemistry, University of Isfahan, Isfahan 81746-73441, Iran

[b] Institute of Physics, Polish Academy of Sciences, Al. Lotników 32/46, 02-668 Warsaw, Poland

Abstract

A diastereomeric pair (homochiral and heterochiral) of Schiff base dioxo molybdenum complex was synthesized using chiral ligand (**HL**: *R*/*S*-1-((naphtalen-3-yl)methylenamino)propan-2-ol) in racemic form. Then, to separation of this diastereomeric pair, crystallization method was proposed which was successful with acetonitrile. ^{1}H NMR technique was used to confirm the results. The complexes thoroughly characterized using FT-IR, elemental analysis, ^{1}H NMR and ^{13}C NMR techniques, and **$MoO_2L(LH_2)^1$** has been structurally characterized using single-crystal X-ray diffraction. The cytotoxic activity of the new compounds has been evaluated using MCF-7 (human breast adenocarcinoma) and HeLa (human cervix adenocarcinoma), in addition to normal human fibroblast cells using the MTT cytotoxicity assay. Compounds **$MoO_2L(LH_2)^1$** and **$MoO_2L(LH_2)^2$** revealed IC50 values 18 μM and 37 μM on MCF-7 and 58 μM and 17 μM on HeLa, respectively. **$MoO_2L(LH_2)^2$** showed high selectivity (3–13 folds) for cancerous cells over normal cells, as the maximum cell mortality of 8.77%. Furthermore, The HSA- and DNA-binding of the Mo(VI) complexes were investigated by absorption, emission spectroscopy, viscosity measurements and molecular docking. Their binding constant are calculated as: HSA-binding of **$MoO_2L(LH_2)^1$** is $6.7 \times 10^4\ M^{-1}$ and of **$MoO_2L(LH_2)^2$** is

$5.8 \times 10^4\ M^{-1}$, while their DNA-binding are $5.6 \times 10^4\ M^{-1}$ and $2.2 \times 10^5\ M^{-1}$, respectively. Their thermodynamic parameters were also determined at different temperatures.

Keywords

Dioxo Mo(VI) Schiff base complex

Diastereomers separation

In vitro assay

HSA binding

DNA binding

1. Introduction

Chiral compounds are of continued interest and have been used widely in pharmaceutical research. It can be because of stereoselective interaction of chiral drugs and also their potent binding with biotargets viz., DNA, as nature of the biomacromolecules is chiral [1]. Therefore, synthesis of chiral compounds is a strategy for synthesis more effective and selective anticancer drugs. Benedetti et al. investigated the biological activity of cisplatin containing chiral ligand and confirmed the importance of chirality [2]. A large number of papers have been published about chiral metal complex in different fields including asymmetric catalyst, biological systems [3], pharmaceutical agent [4] and their anticancer activity [5], [6], [7], [8].

Our research group interest is in the field of synthesis novel Schiff base ligands and complexes [9], [10]. Moreover, we have recently paid attention to biological activities of Schiff base compounds [11], [12]. In particular, we have reported a chiral vanadium complex as a potent anticancer agent [13]. In the present study, in continuation of previous work [13], a chiral Schiff base ligand in racemic form (**HL**: *R*/*S*-1-((naphtalen-3-yl)methylenamino)propan-2-ol) has been used to synthesis dioxomolybdenum (Mo(VI)) complex in ambient temperature. As shown in Fig. 1, racemic ligand leads to synthesis a diastereomeric pair of metal complex. A mixture of racemic ligand is required to have M-*S*,*R*-L_2 (heterochiral) complex that there are few reports about

them [14], [15], [16], and except previous our work, no report has been found about investigation of its biological application.

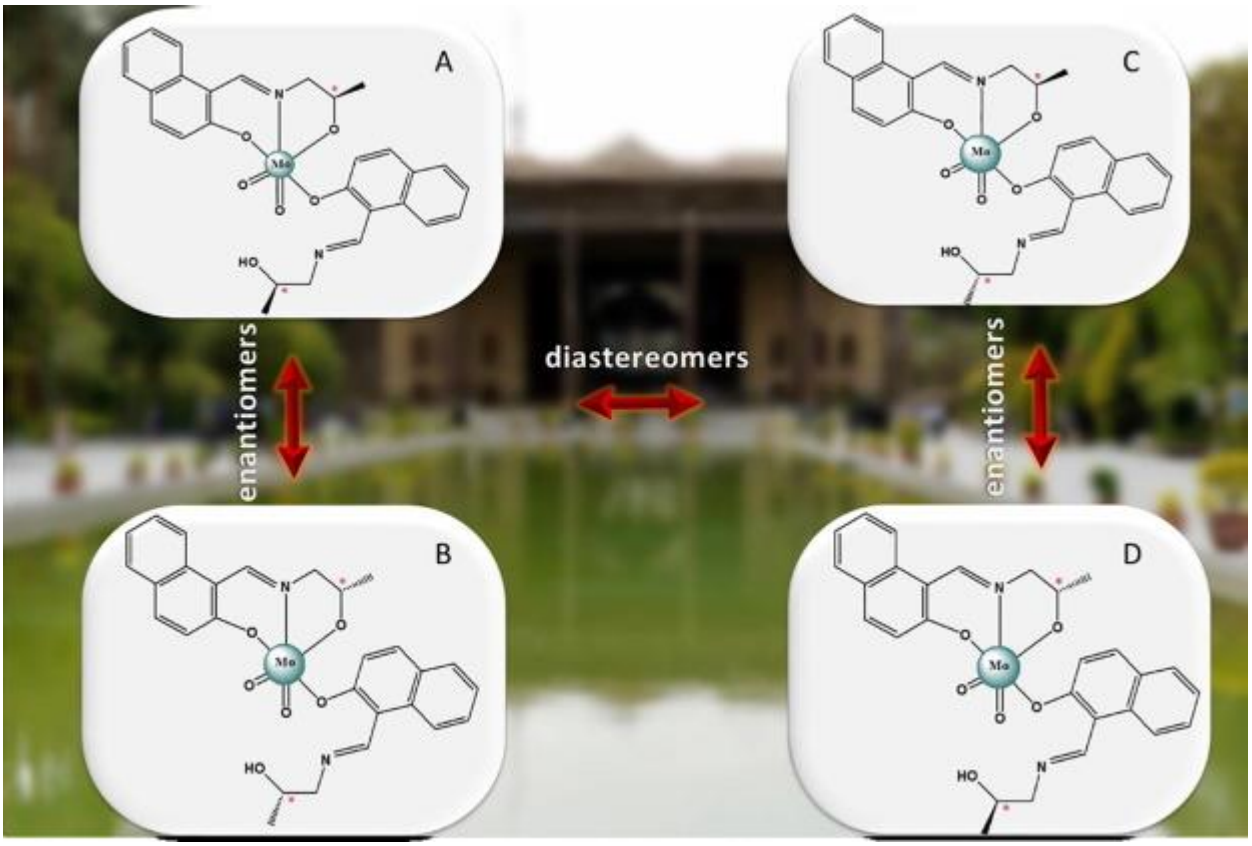

Fig. 1. Four isomers for **$MoO_2L(LH_2)$**.

According to the above, the synthesized Mo complex in this work are in two isomers, homochiral (*R,R*/*S,S*-$MoO_2L(LH_2)$) and heterochiral (*R,S*/*S,R*- $MoO_2L(LH_2)$) forms, named as **$MoO_2L(LH_2)^1$** and **$MoO_2L(LH_2)^2$**, respectively. Herein, we accomplished separation of these isomers by crystallization as a very simple method. Both diastereomers have been characterized by FT-IR, ^{1}H NMR, ^{13}C NMR and elemental analysis and the structure of complex was determined by single crystal X-ray analysis. During this study for the first time a comparative study on *in vitro* cytotoxic activity of two diastereomers against human cell lines (MCF-7 and HeLa) was carried out. Their DNA- and HSA-binding have been evaluated by means of both experimental (fluorescence quenching and UV–Vis spectroscopy methods) and computational methods (molecular docking). In addition, the DNA-binding mode of the complexes was investigated by viscosity measurement.

2. Experimental

2.1. Chemicals and instrumentation

Human serum albumin (HSA), fish sperm DNA (FS-DNA), Tris(hydroxymethyl)-aminomethane (Tris), ethidium bromide (3,8-diamino-5-ethyl-6-phenylphenanthridinium bromide, EthBr), RPMI-1640 medium, antibiotics (penicillin-streptomycin) solution, Fetal bovine serum (FBS) and 3-(4,5-Dimethylthiazol-2-yl)-2,5-Diphenyltetrazolium Bromide (MTT) were purchased from Sigma-Aldrich. 2-Hydroxy-1-naphtaldehhyde and (*R*/*S*)-1-aminopropan-2-ol were obtained from Merck Co. and used without further purification. All salts used for buffer preparation were analytical grade and were dissolved in double distilled water. All of the solutions were used freshly after preparation. The FT-IR spectrum was recorded on a JASCO, FT/IR-6300 spectrometer (4000–400 cm^{-1}) in KBr pellets. ^{1}H and ^{13}C NMR spectra were recorded on a Bruker Avance III 400 spectrometer using DMSO as solvent. The elemental analysis was performed on Leco, CHNS-932 and Perkin-Elmer 7300 DV elemental analyzers. The UV–Vis spectra were recorded on a JASCO V-670 spectrophotometer. Fluorescence measurements were carried out on Shimadzu RF-5000 spectrofluorometer at room temperature. Viscosity was measured using a Brookfield rotational viscometer at room temperature.

2.2. Preparation of Mo(VI) complex

A solution of 2-hydroxy-1-naphtaldehyde (0.1 g, 0.58 mmol) in ethanol was slowly added to a solution of (*R*/*S*)-1-aminopropan-2-ol (0.045 ml, 0.58 mmol) in the same solvent and the mixture was stirred for 4 h in ambient temperature. Then, in the presence of triethylamine (0.125 ml, 0.87 mmol), $MoO_2(acac)_2$ (0.094 g, 0.29 mmol) in absolute ethanol was added (Scheme 1). The resulting mixture was stirred for 6 h to proceed completely in ambient temperature. Whereupon, the complex that separated out was filtered and washed several times.

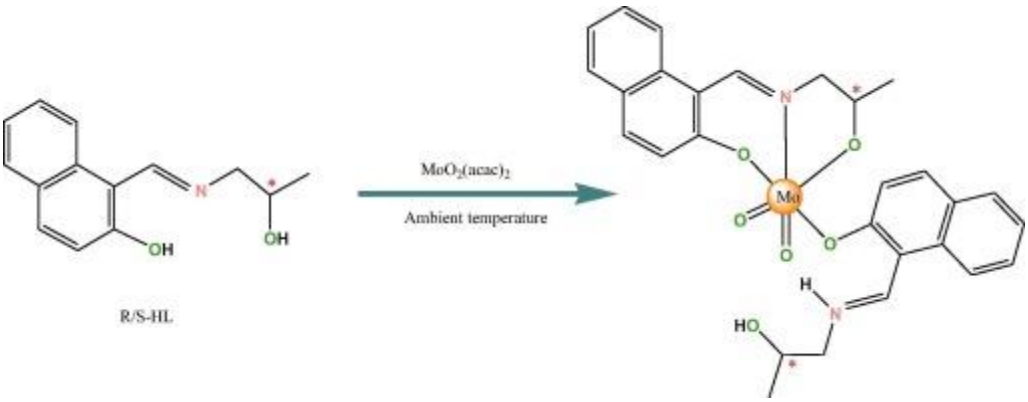

Scheme 1. Synthesis of Mo(VI) complex.

There are four different configurations (Fig. 1A–D) from the synthesized complex. Isomers A and C are enantiomers of B and D, respectively. The enantiopure *R*- or *S* chelate ligand leads to the formation of enantiomeric pair of the type *R,R*-$MoO_2L(LH_2)$ and *S,S*-$MoO_2L(LH_2)$ (Fig. 1 A and B), while racemic ligand (*R*/*S*-**HL**) gives all four isomers.

In our work, the resulting powder was the mixture of two diastereomers, (*R,R*/*S,S*) $MoO_2L(LH_2)$ and (*R,S*/*S,R*) $MoO_2L(LH_2)$, which in this paper are named as **$MoO_2L(LH_2)^1$** and **$MoO_2L(LH_2)^2$**, respectively. Separation of these diastereomers was tested with different solvents that was successful with acetonitrile, and as a result two yellow and orange powders were produced. The slow evaporation solution of the **$MoO_2L(LH_2)^1$** complex gave yellow crystals suitable for crystallography. The typical yield was 78%. *Anal.* Calc. for $C_{28}H_{28}MoN_2O_6$: C: 59.71, H: 5.01, N: 4.49. Found: C: 62.60, H: 4.32, N: 5.07%. Selected IR data (KBr, cm^{-1}): **$MoO_2L(LH_2)^1$**: 1636 (νC N), 1487 (νC N), 1335 (νC O), 878 (ν_{asym}(O Mo O)) and 906 (ν_{sym}(O Mo O)); and **$MoO_2L(LH_2)^2$**: 1634 (νC N), 1458 (νC N), 1334 (νC O), 880 (ν_{asym}(O Mo O)) and 907 (ν_{sym}(O Mo O)). ^{1}H NMR (DMSO-d_6, δ in ppm): **$MoO_2L(LH_2)^1$**: 1.12, 1.31 (d, CH_3), 3.50, 3.65 (dd, C*H*H), 3.75, 4.38 (dd, CH*H*), 3.85, 4.54 (m, CH), 5.05 (s, OH), 6.69–8.40 ($H_{aromatics}$), 8.97, 9.61 (s, H_{imine}), 13.92 (s, NH), and **$MoO_2L(LH_2)^2$**: 1.13, 1.32 (d, CH_3), 3.50, 3.65 (dd, C*H*H), 3.75, 4.38 (dd, CH*H*), 3.95, 4.64 (m, CH), 5.07 (s, OH), 7.07–8.40 ($H_{aromatics}$), 8.98, 9.61 (s, H_{imine}), 13.94 (s, NH). Decomposition point: 191.1 °C for **$MoO_2L(LH_2)^1$** and 217.2 °C for **$MoO_2L(LH_2)^2$**.

2.3. Single crystal diffraction studies

X-ray data for **$MoO_2L(LH_2)$[1]** were collected on a STOE IPDS-II diffractometer with graphite monochromated Mo Ka radiation. A yellow crystal was chosen using a polarizing microscope and was mounted on a glass fiber which was used for data collection. Data were collected at 298(2) K in a series ω scans in 1° oscillations and integrated using the StöeX-AREA [17] software package. A numerical absorption correction was applied using the X-RED and X-SHAPE [18] software for Mo(VI) complex. The data were corrected for Lorentz and Polarizing effects. The structures were solved by direct methods using SIR2004. The non-hydrogen atoms were refined anisotropically by the full-matrix least-squares method on F^2 using SHELXL [19]. All hydrogen atoms were added at ideal positions and constrained to ride on their parent atoms.

Crystallographic data are listed in Table 2. Selected bond distances and angles are summarized in Table 3.

2.4. DNA binding studies

Using the electronic absorption and fluorescence methods, the binding of the Mo complexes was studied in 50 mM Tris buffer at pH 7.5. The concentration of DNA solution which its purity was confirmed by a ratio of UV absorbance at 260 and 280 nm ($A_{260}/A_{280} = 1.9$), was determined by UV absorbance at 260 nm ($\varepsilon = 6600\ M^{-1}\ cm^{-1}$) [11], [20]. Electronic absorption spectra were performed at 25 °C by fixing the concentration of complexes (1×10^{-5} M), and gradually increasing the concentration of CT-DNA. An equal amounts of DNA solution was added to the blank solution to eliminate its absorbance. For every titration step, the mixture solutions were allowed to incubate for 2 min before recording the related spectra.

Fluorescence spectra of DNA–EthBr complex in the presence of different concentrations of Mo(VI) complexes at temperatures 295, 303 and 311 K were studied, according to previous works [21], [22]. The fluorescence quenching experiment was carried out using quartz cuvette with 1 cm optical path length. The excitation wavelength was set to 520 nm, and the emission spectra were recorded in the range of 550–700 nm. In each measurement, the complex–DNA solutions were allowed to incubate for 2 min before recording.

Viscosity experiments were carried out using an ALPHA L Fungilab rotational viscometer and the measurements were performed at 200 rpm at room temperature. The viscosity of a DNA solution was measured with the addition of the Mo(VI) complexes.

2.5. HSA binding experiment

Absorption titration experiment and fluorescence quenching experiment were performed to investigate the HSA-binding of the complexes. To this aim, a stock solution of HSA was prepared in 50 mM phosphate buffer (pH 7) and stored at 4 °C in the dark. Its concentration was determined by UV–Vis spectrophotometry using the molar absorption coefficient 35700 M^{-1} cm^{-1} at 278 nm [11].

The UV–Vis absorption and fluorescence spectra of the HSA solution in the absence and presence of various amounts of Mo(VI) complexes were recorded after 2 min incubation. The fluorescence intensity was measured with excitation wavelength at 295 nm and emission wavelength rang of 300–450 nm. The spectra were recorded at four different temperatures (298, 305, 311 and 315 K). The absorptions of HSA at the excitation and emission wavelengths is approximately zero in all concentrations. Hence, a reduction in the emission intensity is independent of the inner filter effect. Furthermore, all intensities were corrected for the dilution effect in fluorescence and UV absorption experiments for DNA- and HSA-binding.

2.6. Molecular docking simulation

In this work, docking study was carried out to indicate the DNA and HSA-binding site for the synthesized complexes. The 3D structures of (*R,R*)-**$MoO_2L(LH_2)$** complex was generated using the CIF files of its X-ray crystal structures. The CIF files were converted to the PDB format by using the Mercury software (http://www.ccdc.cam.ac.uk/). The optimized structure of **$MoO_2L(LH_2)^2$** complex was calculated using GAUSSIAN 09 [23] at the levels of B3LYP/LANL2DZ. The known crystal structure of DNA (PDB ID: 423D) with sequence d(ACCGACGTCGGT)2 and HSA (PDB ID: 1AO6) were taken from the Brookhaven Protein Data Bank (http://www.rcsb.org/pdb) at resolution of 1.60 and 2.5 Å, respectively. Water molecules of the .pdb files were removed, missing hydrogen atoms and Gasteiger charges were added. Flexible-ligand docking was performed by AutoDock 4.2 molecular-docking program using the implemented empirical free energy function and the Lamarckian Genetic Algorithm [24]. The Gasteiger charges were added to prepare the macromolecule input file for docking and the Auto Grid was used to calculate Grids. A blind docking with 126 lattice points along *X*, *Y*, and *Z* axes was performed to find the active site of ligands to the biomacromolecules. After determination of the active site, the dimensions of the grid map were selected 60 points with

a grid point spacing of 0.375 Å, to allow the ligand to rotate freely. 200 docking runs with 25,000,000 energy evaluations for each run were performed.

2.7. In vitro anticancer activity evaluation

The anticancer activity of the complexes was investigated on human breast (MCF-7) and cervical (HeLa) cancer cell lines as well as normal human fibroblast cells using MTT assay as described previously [25], [26]. The cells were first cultured in RPMI-1640 medium supplemented with 10% FBS and 1% antibiotics solution, and maintained in a humidified 5% CO_2 incubator at 37 °C for two weeks. The cells were then seeded at a density of 10^4 cells per well into the sterile 96 well plates containing 200 µL of the same medium and incubated again at the same condition for 24 h. Following 48 h incubation of the cells with various concentrations of the compounds (0, 1, 5, 10, 20, 50 and 100 µM), the medium was discarded and 100 µL MTT solution (0.5 mg per mL in media) was added to each well and the plates were incubated at 37 °C with 5% CO_2 for 4 h. Subsequently, the culture medium was carefully removed while the formazan crystals were dissolved in 100 µl DMSO and absorbance was measured at 570 nm using micro-plate reader. The cultured cells in the same condition but without treatment were served as control. Three independent experiments were conducted for each toxicity endpoint. The cell viability was determined as ratio of absorbance values from each treatment and the control. The changes in morphology of the cells after exposure to the corresponding concentrations of the compounds were also investigated by using the optical microscope.

3. Result and discussion

In this study, a diastereomeric pair of dioxo molybdenum Schiff base complex was synthesized using racemic ligand, preparing by simple condensation reaction of 2-hydroxy-1-naphtaldehyde and (*R*/*S*)-1-aminopropan-2-ol at ambient temperature. In our synthesis, dioxo molybdenum complex has free functional groups that provides the possibility for linkage of the complex on an insoluble support. Therefore, this complex can be used as heterogeneous catalyst.

3.1. IR spectra

Characteristic IR bands and their assignments are given in Section 2. In the FT-IR spectra of the complexes the absence of the phenolic O H vibration is indicative of deprotonation of ligand to coordination through oxygen atom. The stretching band of the coordinated imine group (C N) appeared at 1636 and 1634 cm^{-1} for **$MoO_2L(LH_2)^1$** and **$MoO_2L(LH_2)^2$** complexes, respectively [11] which shifted to lower frequency compared to the free ligand. This result is indicative of coordination of the metal to the imine nitrogen [27]. The strong bands related to the C $O_{phenolic}$ and C N stretching were observed at the region of 1335 and 1487 cm^{-1} for **$MoO_2L(LH_2)^1$**, 1334 and 1458 cm^{-1} for **$MoO_2L(LH_2)^2$** complexes. The stretching frequencies at about 1186 cm^{-1} were attributed to the coordinated C $O_{alcholic}$ group.

The presence of several medium intensity bands between 2800 and 3300 cm^{-1} in the spectra of Mo(VI) complexes suggests the existence of C H stretching vibrations of aliphatic and aromatic protons. In addition, two sharp bands at 878 cm^{-1} and 880 cm^{-1} in **$MoO_2L(LH_2)^1$** and **$MoO_2L(LH_2)^2$** complexes, respectively, is due to the asymmetric O Mo O stretches and also their symmetric O Mo O stretches are appeared in 906 and 907 cm^{-1}. They are attributed to the vibration of the two double-bonded *cis*-oxygen atoms at the molybdenum core [28], [29]. This results indicate the presence of the MoO_2^{+2} group in *cis* position.

Also, it should be noted that, in the IR spectrum of dinuclear complex the band at about 780 cm^{-1} is indicative of intermolecular metal…oxygen interaction. Absence of the such band in **$MoO_2L(LH_2)^1$** and **$MoO_2L(LH_2)^2$** confirms the monomeric structure of Mo complexes. The IR spectra of compounds also exhibit a broad absorption band in ~3300, characteristic of the stretching vibration of the alcoholic OH group. The remaining frequencies in the IR spectra are due to the vibrations within the ligands.

3.2. NMR spectra

Nuclear magnetic resonance (NMR) can be applied to calculate diastereomeric ratio in a mixture by the integration of characteristic signals with different chemical shifts for diastereomers [30], [31]. Herein, we study characterization and separation of two diastereomers (**$MoO_2L(LH_2)^1$** and **$MoO_2L(LH_2)^2$**) without need to molecular interactions with reagents, chromatography columns and *etc.* [30].

Separation of the diastereomers by crystallization in several solvents was tested, finally it was successful with acetonitrile which suggests different solubility properties of isomers. Complexes **$MoO_2L(LH_2)^1$** and **$MoO_2L(LH_2)^2$** have slight difference in ^{1}H NMR spectra.

The appearance of distinct signals for protons in ^{1}H NMR confirmed the successful separation of diastereomers. As expected, the NMR spectra of the diastereomeric complexes (**$MoO_2L(LH_2)^1$** and **$MoO_2L(LH_2)^2$**) exhibited different stereochemistry at the CH_3 which shows little differences in the chemical shift. The related signals of ^{1}H and ^{13}C NMR experiments were listed in Table 1.

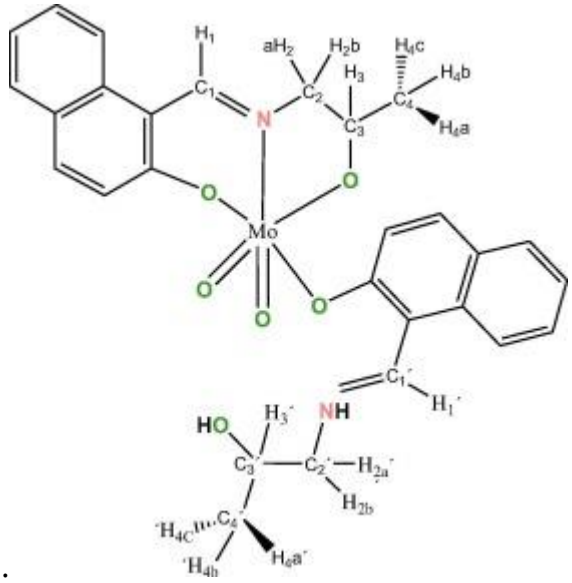

Table 1. ^{1}H and ^{13}C NMR of Mo (VI) complexes.

Empty Cell	**^{1}H NMR**		Empty Cell	**^{13}C NMR**	
	$MoO_2L(LH_2)^1$	**$MoO_2L(LH_2)^2$**		**$MoO_2L(LH_2)^1$**	**$MoO_2L(LH_2)^2$**
OH	5.05	5.07	C_1, C_1'	162.45, 178.43	163.13, 178.43
NH	13.92	13.94	C_2, C_2'	67.15, 77.00	67.07, 77.01
H_1, $H_{1'}$	8.97, 9.61 (s)	8.98, 9.61 (s)	C_3, C_3'	57.49, 65.28	57.47, 65.22
H_{2a}, $H_{2a'}$ H_{2b}, $H_{2b'}$	3.50, 3.65,3.75, 4.38 (dd)	3.50, 3.65,3.75, 4.38 (dd)	C_4, C_4'	19.71, 20.78	19.72, 20.77
H_3, $H_{3'}$	3.85, 4.54 (m)	3.95, 4.64 (m)	$C_{aromatics}$	159.29–105.40	159.24–105.36
H_{4a}, H_{4b}, H_{4c} $H_{4a'}$, $H_{4b'}$, $H_{4c'}$	1.12, 1.31	1.13, 1.32			
$H_{aromatics}$	6.69–8.40	7.07–8.40			

A characteristics feature of the ^{1}H NMR spectra of complexes is the imine proton resonance, observing at 9.61 and 8.97 ppm for **$MoO_2L(LH_2)^1$**, 9.61 and 8.98 for **$MoO_2L(LH_2)^2$**. The resonance signal corresponding to phenolic (O*H*) proton disappears in the Mo(VI) complexes, indicating the coordination of oxygen atom to Mo(VI) ion. The signal at about 5 ppm which is due to CO*H* is observed in the complexes spectra. This means that this oxygen exists at uncoordinated to Mo(VI), as can be seen in X-ray structure (see Section 3.3). In addition, there is a singlet signal at 13.92 and 13.94 ppm in the spectra of **$MoO_2L(LH_2)^1$** and **$MoO_2L(LH_2)^2$**, respectively. It can be due to the existence of an uncoordinated imino nitrogen in their structures which is protonated (see Section 3.3).

The protons of CH*H* are diastereotopic ones, therefore they split each other and have different chemical shifts. The related signals are appeared as doublet of doublet, at 3.50, 3.65, 3.75 and

4.38 ppm for both diastereomer. The signals (m, 1H) at 3.85 and 4.54 ppm for **$MoO_2L(LH_2)^1$**, 3.95 and 4.64 ppm for **$MoO_2L(LH_2)^2$** are due to CH. The doublet signals at 1.12 and 1.31 ppm is attributed to the CH_3 for **$MoO_2L(LH_2)^1$**, while these are at 1.13 and 1.32 ppm for **$MoO_2L(LH_2)^2$**. The ^{13}C NMR spectra of Mo(VI) complexes show 28 signals. The peaks observed at 178.43, 162.45 ppm and 178.43, 163.13 ppm are ascribed to the imine carbon atoms of **$MoO_2L(LH_2)^1$** and **$MoO_2L(LH_2)^2$**, respectively. The existence this peak in the spectra of complexes supports the presence of the Schiff base in the complex.

The ^1H and ^{13}C NMR were run immediately after dissolving complexes in DMSO and gave the expected simple spectra, indicating the integrity of the complexes. No epimerization was observed when the solutions left to stand and their NMR spectra were similar to the initial one.

3.3. Description of the crystal structure of $MoO_2L(LH_2)^1$

The molecular structures of **$MoO_2L(LH_2)^1$** (*R,R*-**$MoO_2L(LH_2)$** and *S,S*-**$MoO_2L(LH_2)$**) have been determined by single crystal X-ray diffraction analysis, and the crystallographic data are collected in Table 2. Also, the selected bond lengths and angles are listed in Table 3. The complex crystallizes in space group $\bar{1}$ and a representative ORTEP view of its asymmetric units with the atom-numbering scheme is presented in Fig. 2.

Table 2. Crystal data and structure refinement for **$MoO_2L(LH_2)^1$**.

Empirical formula	$C_{28}H_{28}N_2O_6Mo$
Formula weight	584.46
T (K)	298(2)
λ (Å)	0.71073
Crystal system	triclinic
Space group	$\bar{1}$
Unit cell dimensions (Å, °)	a = 8.7221(17)

	$b = 12.452(19)$
	$c = 12.860(2)$
	$\alpha = 100.52(3)$
	$\beta = 91.70(3)$
	$\gamma = 105.20(3)$
V (Å^3)	1320.7(5) 320.7(5)
Z	2
D_{calc} (Mg/m^3)	1.470
Absorption coefficient (mm^{-1})	0.541
F(0 0 0)	600
θ range for data collection (°)	2.59–24.99
Index ranges	$-10 \leq h \leq 10$
	$-14 \leq k \leq 14$
	$-15 \leq l \leq 15$
Reflections collected	14 280
Independent reflections	4640 [$R_{int} = 0.0577$]
Data completeness (%)	99.8

Refinement method	full-matrix least-squares on F^2
Data/restraints/parameters	4640/0/341
Goodness-of-fit on F^2	0.911
Final R indices [$I > 2\sigma(I)$]	$R_1 = 0.0395$
	$wR_2 = 0.0902$
R indices (all data)	$R_1 = 0.0602$
	$wR_2 = 0.0939$
Largest difference peak and hole (e Å^{-3})	0.622 and −0.364

Table 3. Selected bond distances (Å) and angles (°) for **$MoO_2L(LH_2)$**[1*].

Mo(1)	O(1)	1.983(3)	O(3)	Mo(1)	O(5)	06.16(15)
Mo(1)	O(2)	1.905(3)	O(3)	Mo(1)	O(2)	99.12(14)
Mo(1)	O(3)	1.709(3)	O(5)	Mo(1)	O(2)	99.97(13)
Mo(1)	O(4)	2.280(3)	O(3)	Mo(1)	O(1)	93.40(14)
Mo(1)	O(5)	1.711(3)	O(5)	Mo(1)	O(1)	101.30(13)
Mo(1)	N(1)	2.255(3)	O(2)	Mo(1)	O(1)	151.17(11)

O(4)	C(15)	1.298(4)	O(3)	Mo(1)	N(1)	91.62(14)
O(1)	C(1)	1.344(4)	O(5)	Mo(1)	N(1)	162.18(12)
O(2)	C(13)	1.444(5)	O(2)	Mo(1)	N(1)	75.45(12)
O(6)	C(27)	1.406(6)	C(1)	O(1)	Mo(1)	130.5(3)
N(2)	C(25)	1.291(5)	O(1)	Mo(1)	N(1)	78.35(11)
N(2)	C(26)	1.475(5)	O(3)	Mo(1)	O(4)	166.32(13)
C(24)	C(15)	1.418(5)	C(15)	O(4)	Mo(1)	134.9(2)
C(24)	C(23)	1.453(5)	C(13)	O(2)	Mo(1)	121.1(2)

*

Symmetry transformations used to generate equivalent atoms: 1 −*x*, −*y*, −*z*.

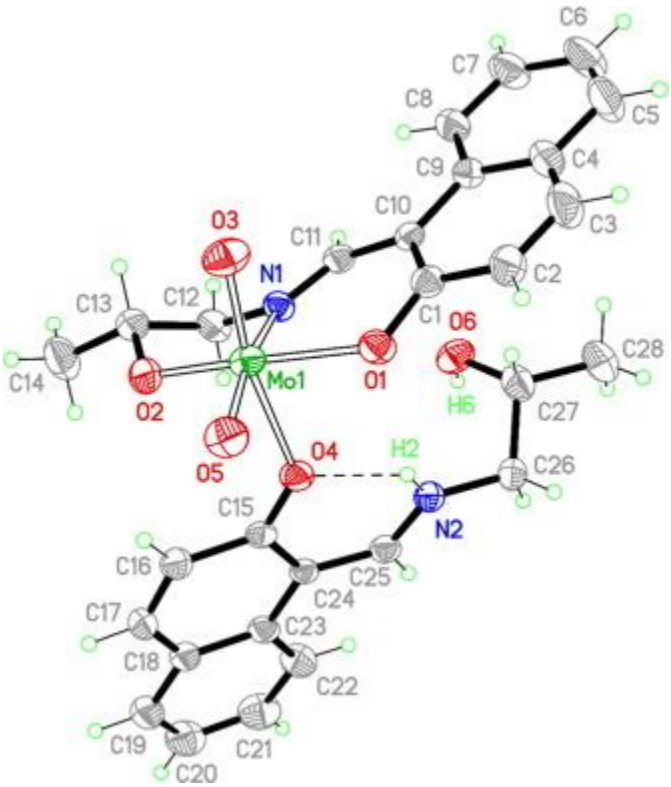

Fig. 2. ORTEP representation of **$MoO_2L(LH_2)^1$**. Displacement ellipsoids are drawn at the 30% probability level and H atoms are shown as small spheres of arbitrary radii. Hydrogen bonds are shown as dashed lines.

The complex contains a stereogenic center at atom C13 (Fig. 2) and the reference molecule was selected as one having the *R*-configuration at atom C13. The centrosymmetric space group confirms that the complex has crystallized as a racemic mixture (Fig. 3).

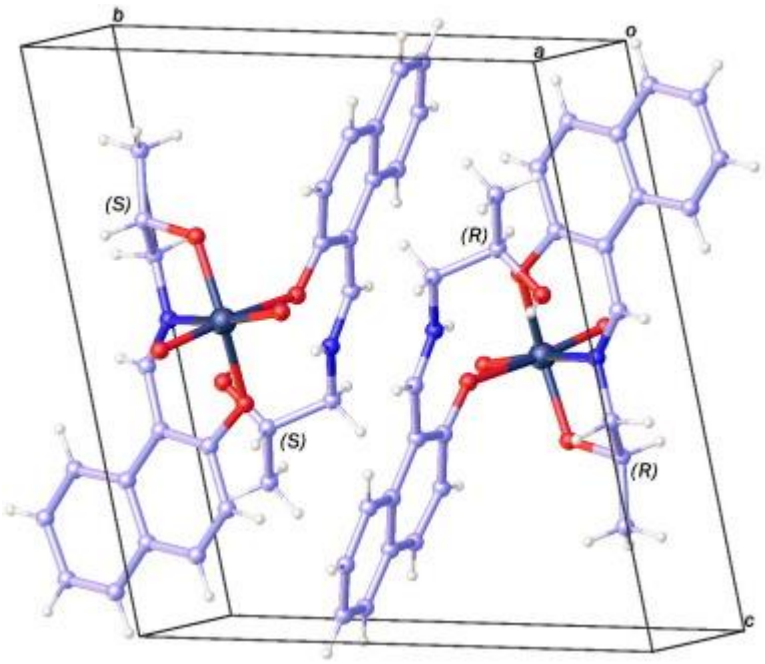

Fig. 3. Racemic mixture (*R,R*-$MoO_2L(LH_2)$ and *S,S*-$MoO_2L(LH_2)$) in unit cell.

The **$MoO_2L(LH_2)$[1]** complex exhibits distorted octahedral geometry consist of a *cis*-$\{MoO2\}^{2+}$ fragment surrounded by two Schiff base ligands, differently, one of the ligands acts as tridentate and another as monodentate ligand. The coordinating sites are occupied by two dioxo oxygen atoms in *cis* arrangement and the remaining four sites are coordinated by two oxygen and one nitrogen atoms of a ligand (L) and one oxygen atom of another ligand (L′). The azomethine N and hydroxyl O atoms of L′ do not participate in coordination and are protonated.

The bond angles in the octahedron differ significantly from the ideal 90°/180° (Table 3). They vary from 75.45(12)° to 106.16(15)° for *cis*-substituted and 151.17(11)°to 166.32(13)° for *trans* substituted, indicating the significance of distortion degree in the octahedron. The bond lengths of complex are comparable with their counterparts in the *cis*-dioxo Mo(VI) complexes [32], [33], [34]. The Mo N(1) and Mo O(4) bond lengths 2.255(3) Å and 2.280(3) Å, respectively are somewhat longer than those for Mo O(1), Mo O(2), Mo O(3) and Mo O(5), 1.983(3), 1.905(3), 1.709(3) and 1.711(3) Å, reflecting the *trans* influence of the oxo ligands. Moreover, the Mo O bond lengths (Mo O3, 1.709(3) Å; Mo O5,

1.711(3) Å) are in the expected range of *cis*-dioxo Mo(VI) complexes [35], [36]. The C N bond distances are 1.291(7) Å (N2 C25) and 1.281(4) Å (N1 C11), are similar to those reported previously [28], [37].

Table 4 shows the Mo complexes synthesized with slightly different ligands. In all the cases, there is a tridentate NOO Schiff base ligand coordinating to *cis*-MoO_2^{2+} species. The same scaffolds are marked with red color [38], [39], [40], [41], [42], [43]. As shown, in our complex and complex **1**, two Schiff base ligands were coordinated to Mo(VI) [44], [45]. Although, their synthetic procedures were completely different. In synthesis of complex **1**, $MoO_2(Sal)_2$ was used instead of $MoO_2(acac)_2$ that we were used. Intermolecular hydrogen band between oxo (Mo O) and hydroxyl (OH) group in both our complex and complex **1** formed 1D chain.

Table 4. The Mo(VI) complexes with similar structure.

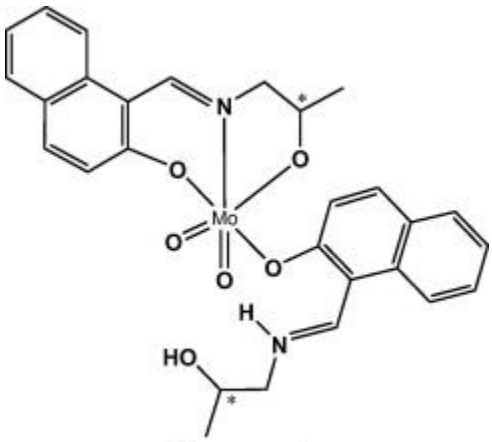

Our complex

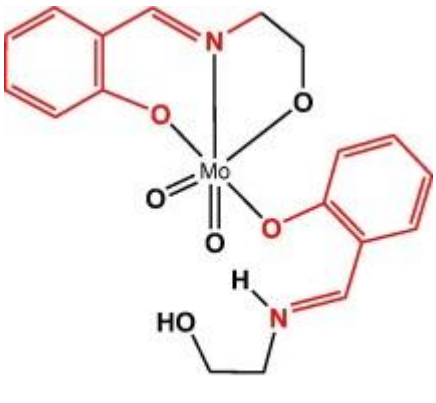

1 [44, 45]

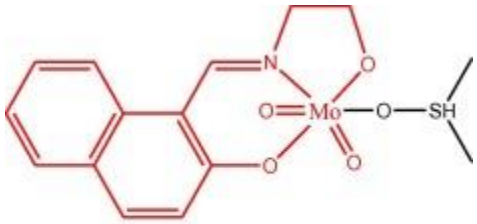

2 [38]

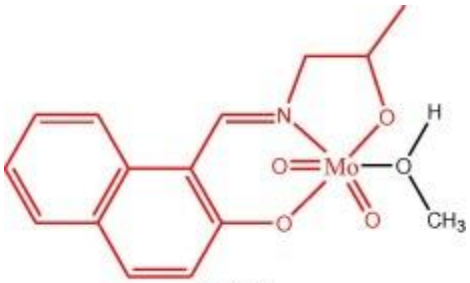

3 [39]

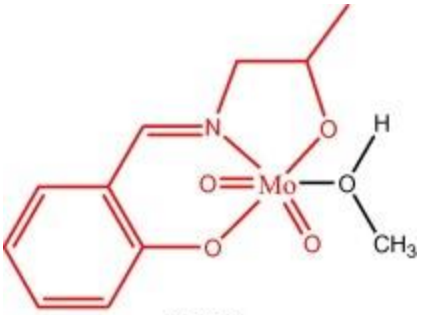

4 [40]

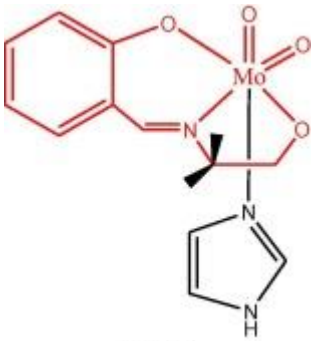

5 [41]

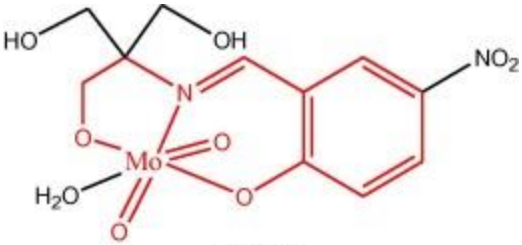

6 [42]

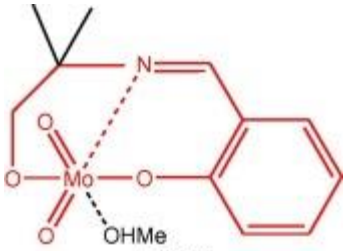

7 [43]

In other complexes, there is one coordinated ligand to Mo(VI) and in their structures, excluding complex **5**, solvent of the reaction (H_2O, MeOH and DMSO) occupies one of the coordination site. In complex **5**, imidazole coordinated to Mo instead of solvent. But in reported complex in this paper, **$MoO_2L(LH_2)$[1]**, two Schiff base ligand coordinated to Mo of *cis*-MoO_2^{2+} species without coordination of any reaction solvents. The most important reason about structural difference between Mo complex in this paper, **$MoO_2L(LH_2)$[1]**, with other reported structures (Table 4) is the use or non-use of triethylamine as base during the reaction. Synthesis of **$MoO_2L(LH_2)$** was carried out in the presence of triethylamine, while in other similar reported structures, the reaction between $MoO_2(acac)_2$ and Schiff base ligands was done without triethylamine as base. Triethylamine is able to change the Ph OH of Schiff base ligand to Ph O^-. In this case, Ph O^- of Schiff base ligand can occupy one of the coordination site of Mo complex in **$MoO_2L(LH_2)$[1]** instead of reaction solvent. The band lengths of **$MoO_2L(LH_2)$[1]** are similar to those seen in related complexes in Table 4. The Mo N (imine) and Mo O (Schiff base ligand) bonds in these complexes are in the range of 2.251–2.293 and 1.93–1.97 Å, respectively.

Also, the complex is chiral at metal center, as shown in Fig. 4, and the absolute configuration of each Mo atom could be determined as either *C* (clockwise) or *A* (anticlockwise) (Fig. 4) using the official nomenclature rules for such compounds [44]. As shown in Fig. 4, ligands

with chirality of *R* and *S* coordinated to Mo atom with *A* and *C* chirality, respectively. On the basis of the above, the two enantiomers in the Fig. 4, can properly be named with the following combinations: S_C, C_{Mo}, S_C and R_C, A_{Mo}, R_C.

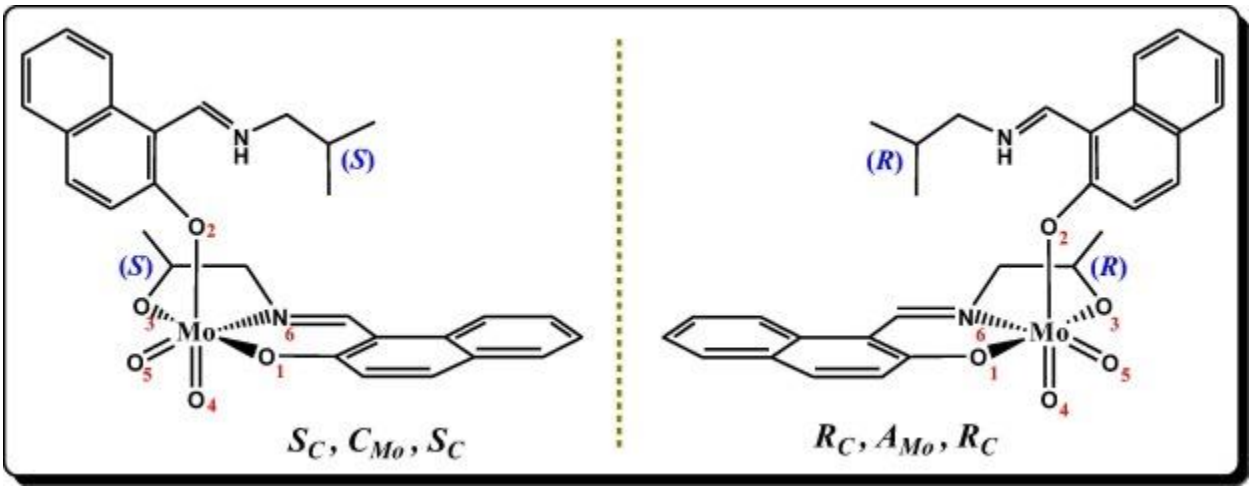

Fig. 4. The two enantiomers of **$MoO_2L(LH_2)^1$** complex, *C* and *A*, with the priority numbers used to define the absolute configuration shown as subscripted indices [44].

The protonated imino nitrogen (N2) forms an intramolecular hydrogen bond with the phenolato oxygen (O4) [N(2) H…O(4)] (Fig. 4). The intramolecular H-bond distances and angle are also in the expected range, (N H: 0.861 Å, H…O: 1.910 Å, N···O: 2.589 Å and NHO: 134.69°) [46], [47], [48]. There is also one intermolecular hydrogen bond of C(6) H(6)…O(3) type in the structure that creates a 1D chain (The inter H-bond geometries: O H: 0.820 Å, H…O: 1.946 Å, N···O: 2.761 Å and NHO: 172.84°). It is noteworthy that the chains have R_C, A_{Mo}, R_C…R_C, A_{Mo}, R_C…R_C, A_{Mo}, R_C or S_C, C_{Mo}, S_C…S_C, C_{Mo}, S_C…S_C, C_{Mo}, S_C configura tions (Fig. 5). According to the hydrogen-bonding classification [49], these intramolecular and intermolecular hydrogen bonding are moderate electrostatic interactions.

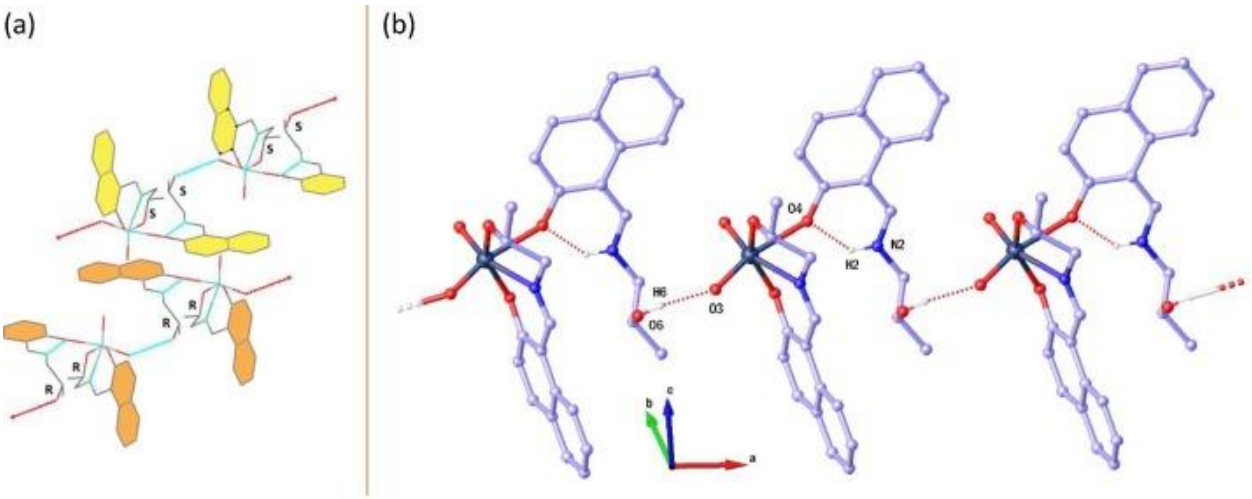

Fig. 5. (a) Illustration of 1D chains formed by O H…O and ligand figuration coordinated to Mo(VI) complex (b) A representation of intramolecular and intermolecular hydrogen bonds in the **$MoO_2L(LH_2)^1$** complex.

The existence coordinated ligand in both *S* and *R* configuration confirms that the diastereomer *R,S*-**$MoO_2L(LH_2)$** is also formed, but its suitable single crystal could not be formed. However, its formation can be confirmed using NMR spectra (see Section 3.2).

3.4. Interaction with DNA

3.4.1. UV–Vis absorption

UV–Vis spectroscopy was used to study about DNA-binding mode and affinity of metal complex to. The absorption spectra of the Mo(VI) complexes show four absorption bands at 303, 322, 392 and 407 nm for **$MoO_2L(LH_2)^1$** and 304, 329, 393 and 412 nm for **$MoO_2L(LH_2)^2$** (Fig. 6). The bands below 330 nm is the result of π–π^* and n–π^* transitions of the ligands and the others ascribed to the metal to ligand charge transfer transitions [50], [51]. Upon the addition of FS-DNA, the complexes show hyperchromism effect which can be due to binding them through groove binding mode and, maybe there is hydrogen bonds between the NH groups of the complexes and N of adenine or O of thymine in DNA [52], [53].

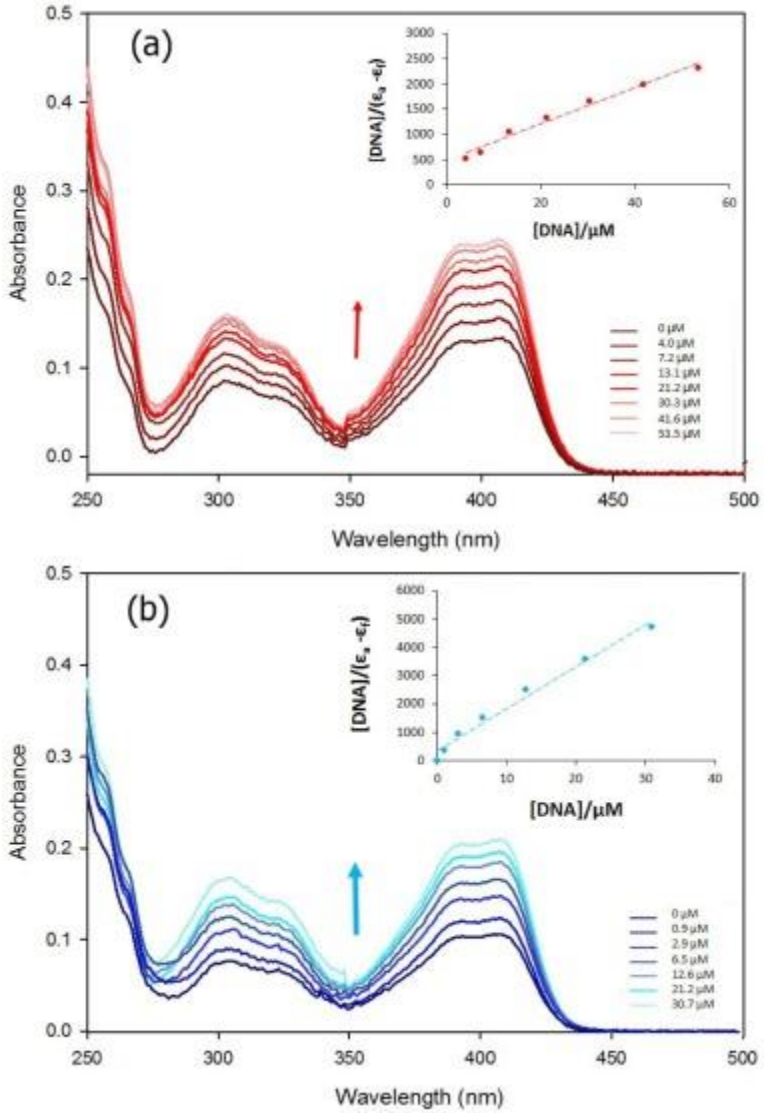

Fig. 6. The change of electronic absorption spectra of (a) **$MoO_2L(LH_2)^1$** and (b) **$MoO_2L(LH_2)^2$** complexes (1×10^{-5} M) upon addition various amounts of FS–DNA (1×10^{-4} M).

The intrinsic binding constant K_b was determined using the Wolf–Shimer equation [52]:

$$\frac{[DNA]}{\varepsilon_a - \varepsilon_f} = \frac{[DNA]}{\varepsilon_b - \varepsilon_f} + \frac{1}{K_b(\varepsilon_b - \varepsilon_f)} \quad (1)$$

where [DNA] is the concentration of FS-DNA; ε_a, ε_f and ε_b are the apparent extinction coefficient, the extinction coefficient for free compounds and the extinction coefficient for the compounds in fully bound form, respectively. ε_f was determined by calibration curve and ε_a is the ratio of A_{obs} to

[compound]. A plot of [DNA]/($\varepsilon_a - \varepsilon_f$) versus [DNA] gives K_b as ratio of slope to y-intercept. The binding constant of FS-DNA with **$MoO_2L(LH_2)^1$** and **$MoO_2L(LH_2)^2$** are determined as 7.6×10^4 and 4.2×10^5 M^{-1}, respectively.

3.4.2. Fluorescence spectroscopy

The emission spectra of the EthBr–DNA complex in the presence of the Mo complexes was used to further investigation of DNA-binding that decreases without any change in the emission λ_{max} (Fig. 7), thereby suggesting the binding of the complexes with DNA.

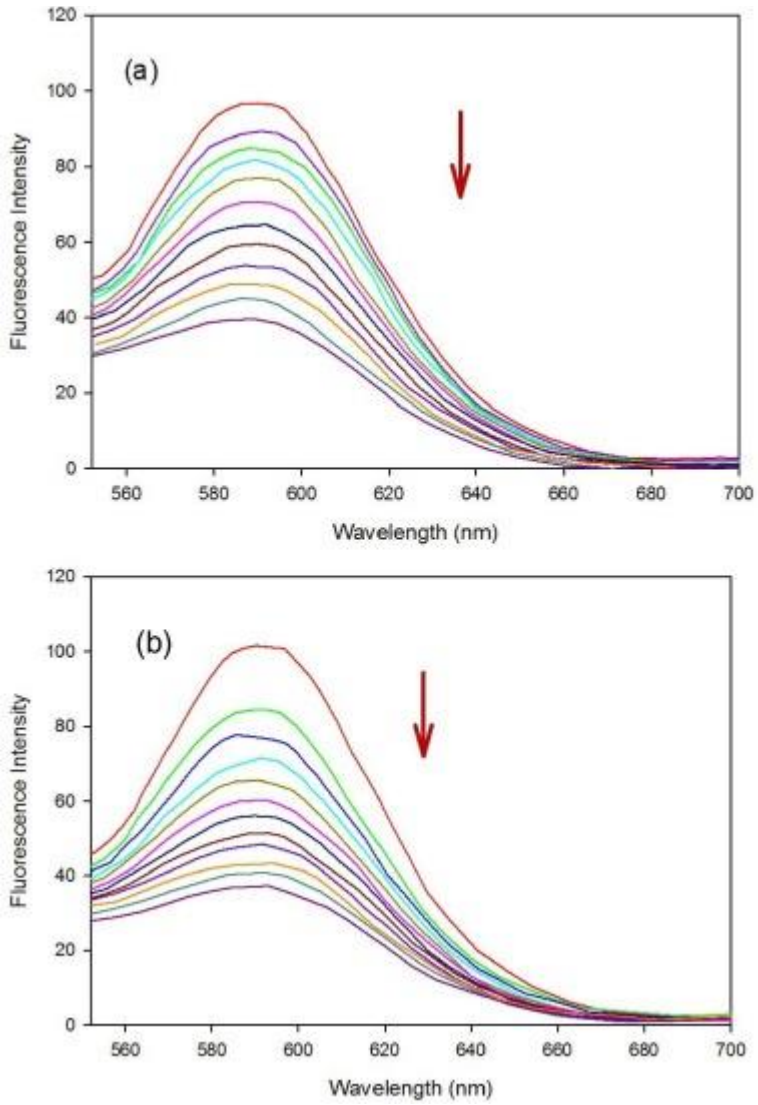

Fig. 7. Fluorescence spectra for titration of DNA:EthBr (50:5 μM) with increasing amounts of (a) **$MoO_2L(LH_2)^1$** and (b) **$MoO_2L(LH_2)^2$** (2.5×10^{-4} M), $\lambda_{ex} = 520$ nm.

The absorptions of the complexes at the excitation and emission wavelengths were approximately zero in all concentrations. Hence, a reduction in the emission intensity is independent of the inner filter effect.

The Stern–Volmer equation was used to define and evaluate binding ability between the complexes and FS-DNA [55]:

$$\frac{F_0}{F} = 1 + K_{sv}[Q] = 1 + k_q \tau [Q] \quad (2)$$

where F_0 and F are the fluorescence intensity of EthBr–DNA complex in absence and presence of the complexes, respectively. [Q] is the concentration of quencher and K_{sv} is the Stern–Volmer quenching constant, k_q is the quenching rate constant of EthBr–DNA and τ is the average lifetime of EthBr–DNA without quencher which is typically equal to 10^{-8} s for biomacromolecules [11]. K_{sv} is determined from the plot of F_0/F versus [Q] (Fig. S1). The values of K_{SV} and k_q were obtained at 295, 303 and 311 K and presented in Table 5.

Table 5. The DNA-binding constant (K_b), the number of binding site (n), the Stern–Volmer constant (K_{SV}) of the compounds and the quenching rate constant of DNA (k_q).

Compounds	***T* (K)**	**K_b (M^{-1})**	**K_{SV} (M^{-1})**	**k_q (M^{-1} S^{-1})**
$MoO_2L(LH_2)^1$	295	5.6×10^4	9.7×10^3	9.7×10^{11}
	303	7.4×10^5	1.2×10^4	2.4×10^{12}
	311	3.3×10^6	2.4×10^4	1.2×10^{12}
$MoO_2L(LH_2)^2$	295	2.2×10^5	1.1×10^4	1.1×10^{12}
	303	1.8×10^4	9.3×10^3	9.3×10^{11}
	311	1.6×10^4	5.2×10^3	5.2×10^{11}

Moreover, binding constant (K_b) of the complexes and FS-DNA can be calculated by this experiment and using following equation [56]:

$$\ln\left(\frac{F_0-F}{F}\right) = \ln K_b + n \ln [Q] \quad (3)$$

"K_b" is obtained from the plot of ln $((F_0 - F)/F)$ versus ln $[Q]$ as a *y*-intercept (Fig. S2). Furthermore, "*n*" which is the number of binding site per nucleic acid is slope of the plot. The intrinsic binding constant (K_b) of the complexes were calculated at different temperatures and presented at Table 5. Investigation of DNA-binding of the complexes in different temperatures can be provide valuable information about the mechanism of fluorescence quenching which is classified into two mechanisms: static quenching and dynamic quenching. In the static mechanism, the fluorophore and the quencher collide together in the ground state while fluorophore and quencher collide together in the excited state in dynamic mechanism [11]. Dynamic and static quenching can be distinguished by their differing dependent on the temperature [57]. As it can be seen in Table 5, a diastereomeric pair shows different behavior with increasing temperature; K_{SV} of **$MoO_2L(LH_2)^1$** increases while that of **$MoO_2L(LH_2)^2$** decreases. These results support that quenching fluorescence in the case of **$MoO_2L(LH_2)^1$** and **$MoO_2L(LH_2)^2$** occurs by dynamic and static mechanism, respectively.

3.4.3. Determination of the thermodynamic parameters

With the objective to assess the effects of temperature on DNA-binding of the complexes and to measure the thermodynamic parameters, the fluorescence experiment was performed at three different temperatures (295, 303 and 311 K). Ross and Subramanian have used the sign and magnitude of the thermodynamic parameters (enthalpy change (ΔH), entropy change (ΔS) and free energy change (ΔG)) to determination of the type of these non-covalent interactions in a variety of host guest systems [28]. From the thermodynamic standpoint, $\Delta H > 0$ and $\Delta S > 0$ imply a hydrophobic interaction; $\Delta H < 0$ and $\Delta S < 0$ reflect the van der Waals force or hydrogen bond formation; and $\Delta H \approx 0$ and $\Delta S > 0$ suggestive of an electrostatic forces. The values of ΔH and ΔS are obtained from the van't Hoff equation [58]:

$$\ln K_b = -\frac{\Delta H}{RT} + \frac{\Delta S}{R} \quad (4)$$

where K_b is the binding constant at the corresponding temperature, T is the absolute temperature in K and R is the gas constant. The values of ΔH and ΔS can be determined from the linear relationship between ln K and the reciprocal absolute temperature. ΔG can be evaluated from the following equation [59]:

$$\Delta G = \Delta H - \mathrm{T}\Delta S \quad (5)$$

Table 6 lists the values of ΔG, ΔH and ΔS. The negative values of ΔG for both complexes and at all temperatures reveal that the DNA-binding process was spontaneous, and the lower ΔG values for **$MoO_2L(LH_2)^2$** indicate its higher binding affinity. The positive ΔH and ΔS values for **$MoO_2L(LH_2)^1$** suggest that hydrophobic interaction played a major role in its DNA interaction. Furthermore, ΔS has dominant role in the interaction between DNA and **$MoO_2L(LH_2)^1$**. In addition, both the negative ΔH and ΔS values make it clear that the van der Waals force and hydrogen bond were the main driving force in the **$MoO_2L(LH_2)^2$**–DNA binding process. In this case the enthalpy term has major role to make ΔG negative. These results were further confirmed by the molecular docking studies.

Table 6. Thermodynamic parameters for interaction of **$MoO_2L(LH_2)^1$** and **$MoO_2L(LH_2)^2$** with DNA.

Compounds	***T* (K)**	**ΔG (kJ mol^{-1})**	**ΔH (kJ mol^{-1})**	**ΔS (J mol^{-1})**
$MoO_2L(LH_2)^1$	295	−27.21		
	303	−33.22	194.74	752.36
	311	−39.25		
$MoO_2L(LH_2)^2$	295	−29.25		
	303	−26.63	−125.92	−327.7

Compounds	*T* (K)	ΔG (kJ mol^{-1})	ΔH (kJ mol^{-1})	ΔS (J mol^{-1})
	311	−24.00		

3.4.4. Viscosity measurement

Changes of length DNA that may occur as a consequence of binding to a small molecule, leads to changes of DNA viscosity. In intercalative mode, base pairs are separated to accommodate the binding ligand, so causes increases of DNA length. Vice versa, groove binding and electrostatic bend the DNA helix, reduces its length and leads to the reduction or no change in the DNA viscosity [60], [61]. The slow decrease in viscosity of DNA with increasing amount of the complexes (Fig. 8) indicates groove binding.

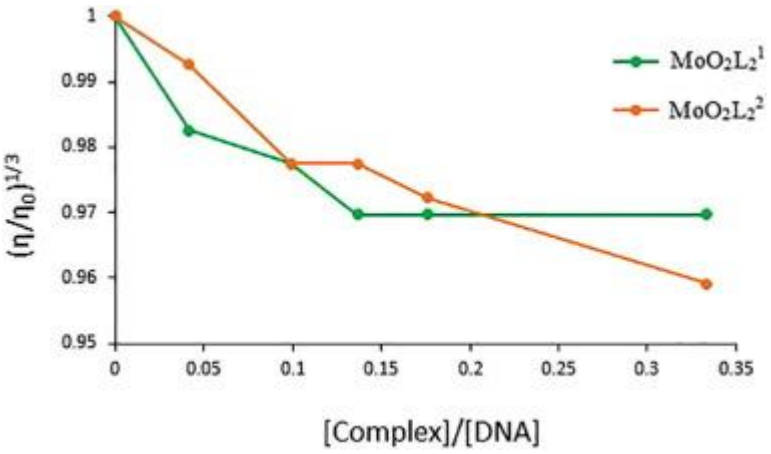

Fig. 8. Effect of increasing amounts of Mo(VI) complexes on the viscosity of DNA. [Complex]/[DNA] = 0, 0.05, 0.1, 0.15, 0.2, 0.3.

The obtained data are presented as $(\eta/\eta^0)^{1/3}$ versus [complex] [54], where η and η^0 are the viscosity of DNA in the absence and presence of the compound, respectively.

The degree of reduction of DNA viscosity, which may depend on affinity of Mo(VI) complexes to DNA, follows the order of **$MoO_2L(LH_2)^1$** < **$MoO_2L(LH_2)^2$**, and it is consistent with UV–Vis and fluorescence results.

3.4.5. Docking study

Investigation of molecular interaction of the Mo(VI) complexes with DNA was carried out through molecular docking studies, suggesting both complexes bind with the minor groove of DNA (Fig. 9).

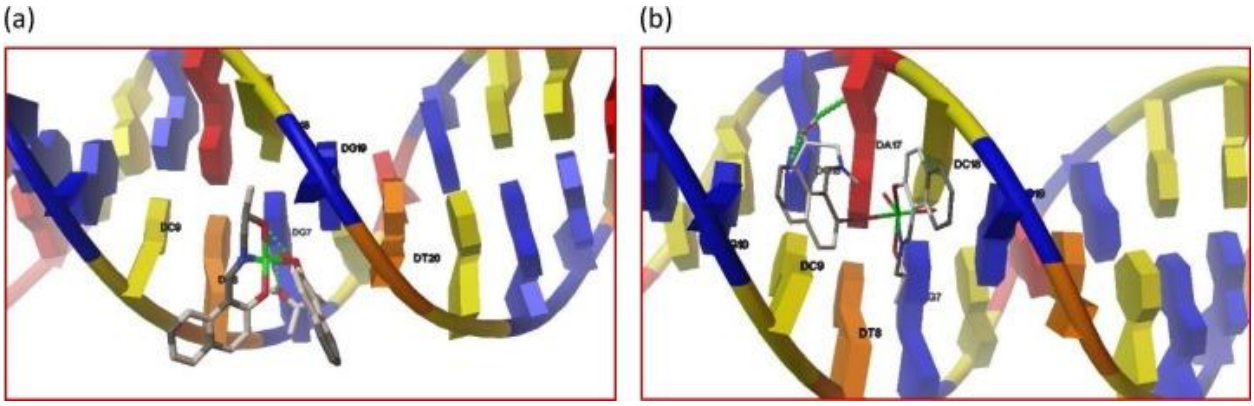

Fig. 9. Molecular docking poses for the interaction of (a) **$MoO_2L(LH_2)^1$** and (b) **$MoO_2L(LH_2)^2$** complexes with the minor groove of DNA.

Based on this data, interaction between **$MoO_2L(LH_2)^1$** with DC18, DT8, DC9, DG19, DT20 and interaction of **$MoO_2L(LH_2)^2$** with DC16, DC9, DG10, DG7, DT8, DC18 is possible. Also, Fig. 9 indicates there are two hydrogen bonds in Mo(VI)–DNA complexes and the binding free energies (ΔG), are obtained −7.36 and −7.66 kcal mol^{-1} for **$MoO_2L(LH_2)^1$** and **$MoO_2L(LH_2)^2$**, respectively. These results revealed the stronger DNA-binding of **$MoO_2L(LH_2)^2$**. This observation is fully supported by experimental results. Also, both the experimental results and computational docking data collectively suggest that the synthesized complexes are DNA groove binder.

3.5. Interaction with human serum albumin (HSA)

3.5.1. UV–Vis absorption

Herein, we have determined the intrinsic binding constant of the complexes to HSA, using UV–Vis absorption spectroscopy. Through addition of various amount of **$MoO_2L(LH_2)^1$** and **$MoO_2L(LH_2)^2$** complexes (5×10^{-5} M), progressive decreases and increases were observed in the absorption peak of HSA at 278 nm, respectively (Fig. 10),

indicative of interaction of the complexes with HSA. Furthermore, the obvious red-shift on the absorption spectra may be accounted for the microenvironment changes of HSA molecule [62].

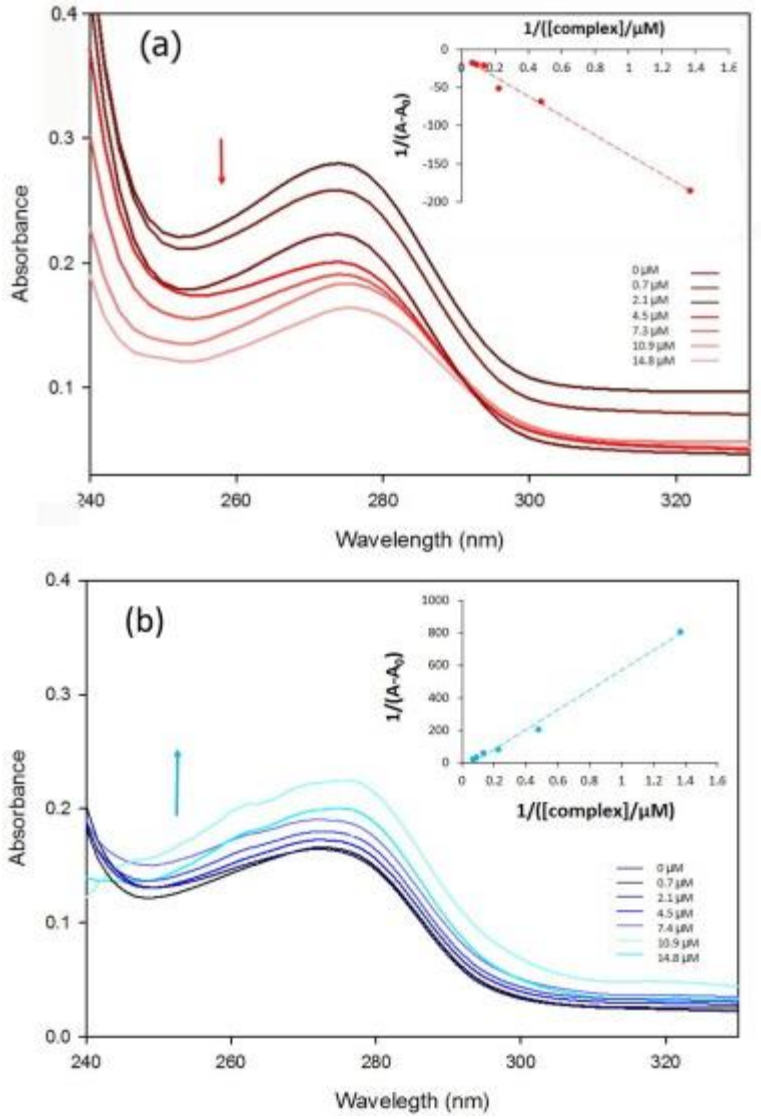

Fig. 10. The change of electronic absorption spectra of HSA upon addition of various amounts of (a) **$MoO_2L(LH_2)^1$** and (b) **$MoO_2L(LH_2)^2$** complexes.

Benesi–Hildebrand plot and the following equation [63], [64] were used to assess the binding ability of the title complexes with HSA.

$$\frac{1}{(A-A_0)} = \frac{1}{(A_{max}-A)} + \frac{1}{K_b(A_{max}-A)} \times \frac{1}{[M]} \quad (6)$$

where A_0 and A are the absorbance of HSA in the absence and presence of drug, respectively. A_{max} is the obtained absorbance at saturation and [M] is the concentration of complex [64]. The plot of 1/(-0) versus1/[]gives K_b as ratio of y-intercept to slop. The binding constants for **$MoO_2L(LH_2)^1$** and **$MoO_2L(LH_2)^2$** are equal to 7.6×10^4 and 6.1×10^4 M^{-1}, respectively (Fig. 9).

3.5.2. Fluorescence spectroscopy

In this work, the fluorescence quenching of 5×10^{-6} M HSA was measured at the presence of various amounts of the Mo(VI) complexes (5×10^{-5} M) at different temperatures (298, 305, 311 and 315 K) (Fig. 11).

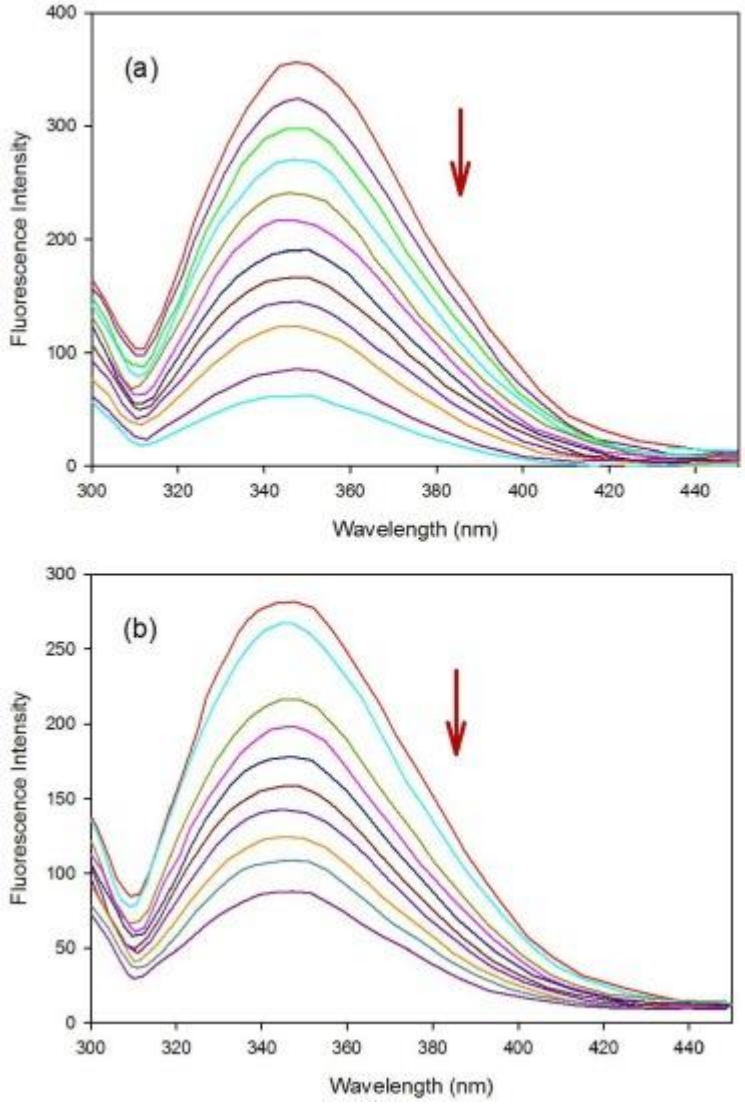

Fig. 11. Fluorescence spectra of HSA (5×10^{-6} M) in the presence of increasing amounts of (a) **$MoO_2L(LH_2)^1$** and (b) **$MoO_2L(LH_2)^2$** (5×10^{-5} M), $\lambda_{ex} = 295$ nm.

The values of K_{SV}, k_q and K_b were obtained at 298, 305, 311 and 315 K and presented in Table 7 (Eqs. (2), (3)) (Fig. S3 and S4) [55], [56]. As it is seen in Table 7, the calculated K_b and K_{SV} values have a direct relation with temperature, hence the quenching mechanism is dynamic for both of the Mo(VI) complexes.

Table 7. The HSA-binding constant (K_b), the number of binding site (n), the stern–volmer constant (K_{SV}) of the compounds and the quenching rate constant of HSA (k_q).

Compounds	***T* (K)**	***K*b (M^{-1})**	***n***	***K*SV (M^{-1})**	***k*q (M^{-1} S^{-1})**
$MoO_2L(LH_2)^1$	298	6.7×10^4	0.95	5.5×10^4	5.5×10^{12}
	305	1.2×10^5	0.75	6.9×10^4	6.9×10^{12}
	311	2.8×10^6	0.57	1.0×10^5	1.0×10^{13}
	315	3.1×10^6	0.60	1.2×10^5	1.2×10^{13}
$MoO_2L(LH_2)^2$	298	5.8×10^4	0.90	3.9×10^4	3.9×10^{12}
	305	1.2×10^5	0.67	6.6×10^4	6.6×10^{12}
	311	1.9×10^5	0.67	8.1×10^4	8.1×10^{12}
	315	2.4×10^5	0.66	9.8×10^4	9.8×10^{12}

3.5.3. Determination of the thermodynamic parameters

The effects of temperature on HSA-binding of the complexes were also investigated and the thermodynamic parameters was measured. Therefore, the fluorescence experiment was performed at four different temperatures (298, 305, 311 and 315 K).

The values of Δ*H*, Δ*S* and Δ*G* were calculated as explained in Section 3.4.3. Table 8 lists the results. In the present case, the positive Δ*H* and Δ*S* values make it clear that the hydrophobic interaction is the main driving force in the Mo(VI) complexes–HSA binding. Also, the negative values of Δ*G* at all temperatures them reveal that the protein binding process is spontaneous and the lower Δ*G* values for **$MoO_2L(LH_2)^1$** indicate its higher affinity for binding to HSA.

Table 8. Thermodynamic parameters for interaction of **$MoO_2L(LH_2)^1$** and **$MoO_2L(LH_2)^2$** with HSA.

Compounds	***T*** **(K)**	**Δ*G*** **(kJ mol^{-1})**	**Δ*H*** **(kJ mol^{-1})**	**Δ*S*** **(J mol^{-1})**
$MoO_2L(LH_2)^1$	295	−102.83		
	305	−105.24	75.41	345.30
	311	−107.32		
	315	−108.70		
$MoO_2L(LH_2)^2$	295	−92.84		
	305	−95.02	65.5	311.77
	311	−96.89		
	315	−98.14		

3.5.4. Energy transfer from HSA to complexes

The fluorescence quenching of HSA upon its binding to metal complex can be indicative of energy transfer between HSA and metal complex. This energy transfer explained by fluorescence resonance energy transfer (FRET) theory, known as Förster's resonance energy transfer which is an interaction between the excited molecule and its adjacent molecule. Upon this interaction, energy absorbed by donor molecule is transferred to an acceptor [65]. According to this theory, three conditions are required to energy transfer: (1) the donor should have fluorescence, (2) the fluorescence emission spectrum of the donor and the UV–Vis spectrum of the acceptor should have sufficient overlap (3) the small distance between donor and acceptor (<8 nm) [65]. The distance and efficiency of energy transfer (*E*) between tryptophan residue of HSA and the complexes has been calculated, using this theory through the following equation:

$$E = 1 - \frac{F}{F_0} = \frac{R_0^6}{R_0^6 + r^6} \quad (7)$$

where R_0 is the critical distance when the transfer efficiency is 50%; r is the distance between donor and acceptor. R_0 can be calculated by Eq. (8) [66].

$$R_0{}^6 = 8.79 \times 10^{-25}\ K^2\ N^{-4}\ J\ \varphi \quad (8)$$

In the above equation, the term K^2 is the orientation factor of the dipoles; N is the refracted index of medium, J is the overlap integral of the fluorescence spectrum of the donor with absorption spectrum of the acceptor and **?** is the fluorescence quantum yield of the donor. The value of J can be calculated by the following expression:

$$J = \frac{\sum F(\lambda)\varepsilon(\lambda)\lambda^4 \Delta\lambda}{\sum F(\lambda)\Delta\lambda} \quad (9)$$

where $F(\lambda)$ is the fluorescence intensity of the donor in the absence of the acceptor at wavelength λ and **?** is the molar absorption coefficient of the acceptor at λ. In the present case, $K^2 = 2/3$, $N = 1.336$ and **?** = 0.15 for HSA. According to Eqs. (7), (8), (9) the values of the parameters for **$MoO_2L(LH_2)^1$** were $J = 3.7 \times 10^{-20}$ cm^3 L mol^{-1}, $R_0 = 0.30$ nm, $E = 0.6$ and $r = 0.28$ nm. The same parameters were calculated for **$MoO_2L(LH_2)^2$** $J = 8.8 \times 10^{-20}$ cm^3 L mol^{-1}, $R_0 = 0.37$ nm, $E = 0.57$ and $r = 0.26$ nm.

Fig. 12 represents the overlap of the fluorescence emission spectrum of HSA (3 μM) and the UV–Vis spectrum of the complexes (3 μM). The values of r for the complexes are less than 8 nm and $0.5\ R_0 < r < 1.5\ R_0$, suggesting energy transfer from HSA to them occurs with high probability [67].

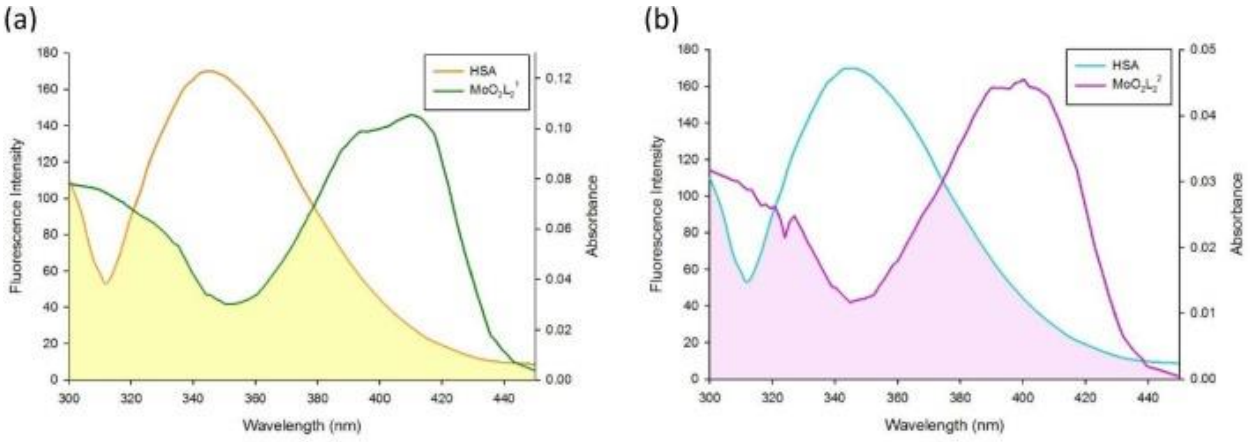

Fig. 12. Spectral overlap of the HSA fluorescence with the absorption spectrum of **$MoO_2L(LH_2)^1$** complex (a) and **$MoO_2L(LH_2)^2$** one (b). [HSA] = [complexes] = 3 μM, λ_{ex} = 295 nm.

3.5.5. Molecular docking of the Mo(VI) complexes with HSA

The Mo(VI) complexes were docked to the crystal structure of HSA and their interaction with HSA was investigated. According to Fig. 13 that is displayed the crystal structure of HSA and its ligand binding sites [68], **$MoO_2L(LH_2)^1$** and **$MoO_2L(LH_2)^2$** complexes were bound to the binding sites at domain IB and cleft, respectively.

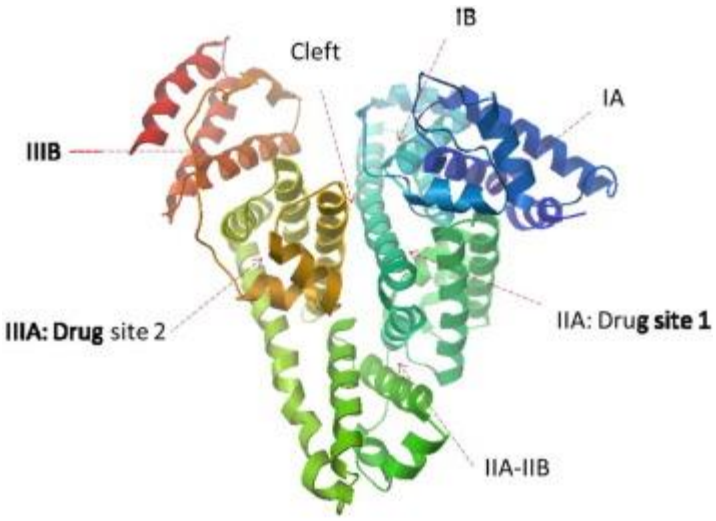

Fig. 13. The ligand binding sites of HSA.

Molecular docking of Mo(VI) complexes with HSA is shown in Fig. 14. As it is clear in this figure, there are two hydrogen bonds between each of Mo(VI) complexes and HSA amino acids, hydrogen bonds between O_{oxo} of **$MoO_2L(LH_2)^1$** and ARG117, hydroxyl group (O6–H6) of **$MoO_2L(LH_2)^1$** and LEU115, O4 of **$MoO_2L(LH_2)^2$** and LYS195, O6 of **$MoO_2L(LH_2)^2$** and LYS436. In addition, there are two π–π interactions between phenyl rings of **$MoO_2L(LH_2)^1$** and TYR161 and TYR138 amino acid residues. While in **$MoO_2L(LH_2)^2$**-HSA complex, there are two π–cation interactions with LYS195 amino acid residue. Also, there are four categories hydrophobic and hydrophilic contacts between the Mo(VI) complexes atoms and the amino acids of the binding site, viz. (i) hydrophobic contacts between **$MoO_2L(LH_2)^1$** atoms and LEU162, LEU185, ILE142 and VAL116, (ii) hydrophilic contacts between **$MoO_2L(LH_2)^1$** atoms and ARG145 and ARG186, (iii) hydrophobic contacts between **$MoO_2L(LH_2)^2$** atoms and ALA191, CYS448 and PRO447, (iv) hydrophilic contacts between **$MoO_2L(LH_2)^2$** atoms and GLU292, LYS436 and ASP451.

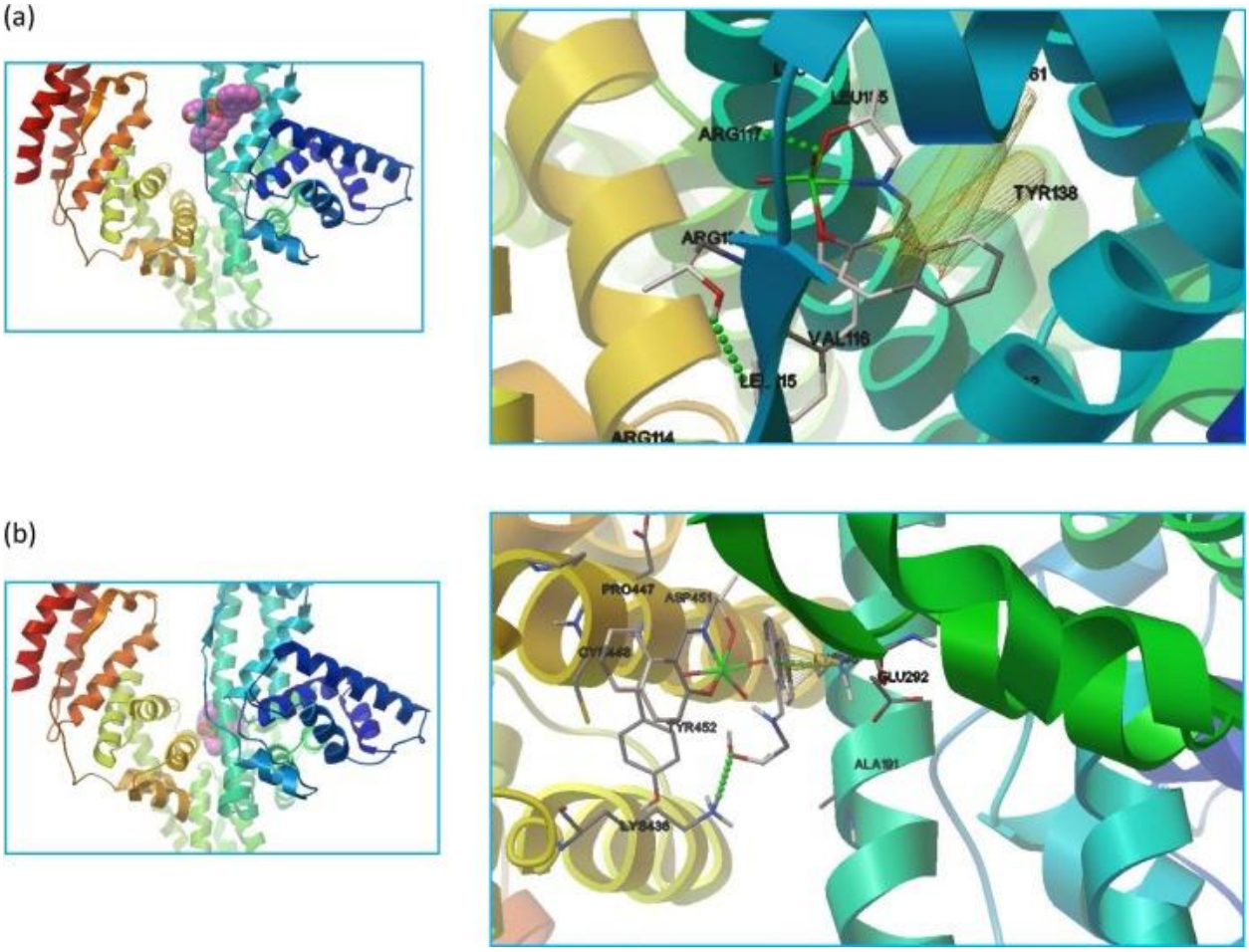

Fig. 14. Docking poses of (a) **$MoO_2L(LH_2)^1$** and (b) **$MoO_2L(LH_2)^2$** in the active site of HSA. (Left) The full view of the complexes docked in HSA; (Right) the interaction mode between the complexes and HSA, the green dashed line, cylindrical and conical shapes show hydrogen bond, π–π and π–cation interactions, respectively. (Color online.)

The binding energy for **$MoO_2L(LH_2)^1$** and **$MoO_2L(LH_2)^2$** complexes with HSA are evaluated about −10.91 and −7.13 kcal.mol^{-1}, respectively. The larger negative value of binding energy for **$MoO_2L(LH_2)^1$** means the higher affinity of it which is in a good agreement with experimental data. As a result, the theoretical and experimental data show slight and considerable difference between binding constants of two diastereomers with HSA and DNA, respectively.

3.6. Cell viability assay

MTT assay was used to elucidate the anti-proliferative potential of Mo(VI) complexes on two carcinoma cell lines including MCF-7 and HeLa and also their adverse effects on normal human fibroblast cells. This colorimetric assay evaluates the viability of cells depending on their metabolic activity by measuring the content of NAD(P)H-dependent oxidoreductase enzymes in the living cells. To the best of our knowledge, it is the first comparative study on the anticancer activity of a diastereomeric pair. The results clearly showed the significant anticancer activity of the compounds depending on the concentration, as the proliferation of cancer cells decreased progressively by increasing the concentration of compounds (Fig. 15).

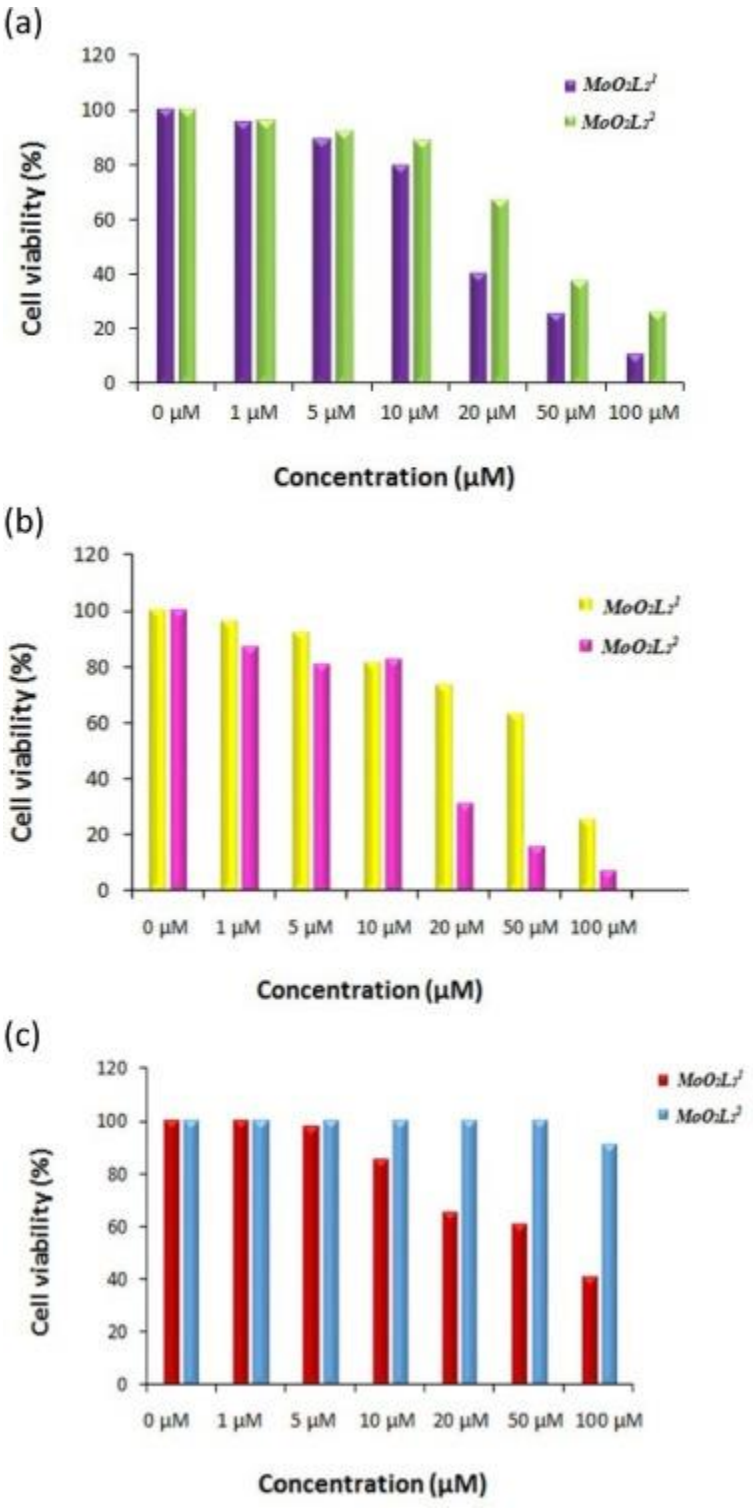

Fig. 15. The viability percentage of (a) MCF-7, (b) HeLa cancer cells and (c) normal fibroblast cells after treatment with different concentrations of Mo(VI) complexes for 48 h.

Interestingly, two diastereomers displayed relatively different effects on cancer cells. The anticancer activity of **$MoO_2L(LH_2)^1$** on MCF-7 cells was more than HeLa cancer cells, while **$MoO_2L(LH_2)^2$** exhibits more cytotoxic on HeLa cells, indicating their cell specific activity (Fig. 15). The maximum mortality of 89.24% MCF-7 cancer cells and 92.75% HeLa cancer cells obtained after 48 h exposure of cancer cells to 100 μM **$MoO_2L(LH_2)^1$** and **$MoO_2L(LH_2)^2$**, respectively.

IC50 values of 18 and 58 μM (in the case of **$MoO_2L(LH_2)^1$**), and 37 and 17 μM (in the case of **$MoO_2L(LH_2)^2$**) obtained for MCF-7 and HeLa cancer cells, respectively. Interestingly, the toxic effects of the compounds on the normal fibroblast cells were significantly less than cancer cells, as the maximum cell mortality of 59.08% and 8.77% obtained after 48 h incubation of fibroblast cells with 100 μM of **$MoO_2L(LH_2)^1$** and **$MoO_2L(LH_2)^2$**, respectively. The results clearly indicate the promising and specific anticancer activity of these diastereomers, especially **$MoO_2L(LH_2)^2$**. In a relative study, Feng *et al.* (2012) reported the dose dependent anticancer activity of molybdenum(VI) complexes, as maximum inhibition ratio of approximately 90% obtained for six kinds of human cancer cell lines by increasing the concentration of complexes to 100 μg/mL (about 200 μM) [69].

Optical microscopic studies also used to further evaluate the cytotoxicity of compounds. The results showed the significant morphological changes of cancer cells following exposure to the synthesized Mo(VI) complexes. The changes in cell morphology were different based on the compound and cell line which confirm the results of MTT assay. These morphological changes predominantly include cell shrinkage and rounding following with the suppression of cell growth and finally the cell clumping and death (Fig. 16).

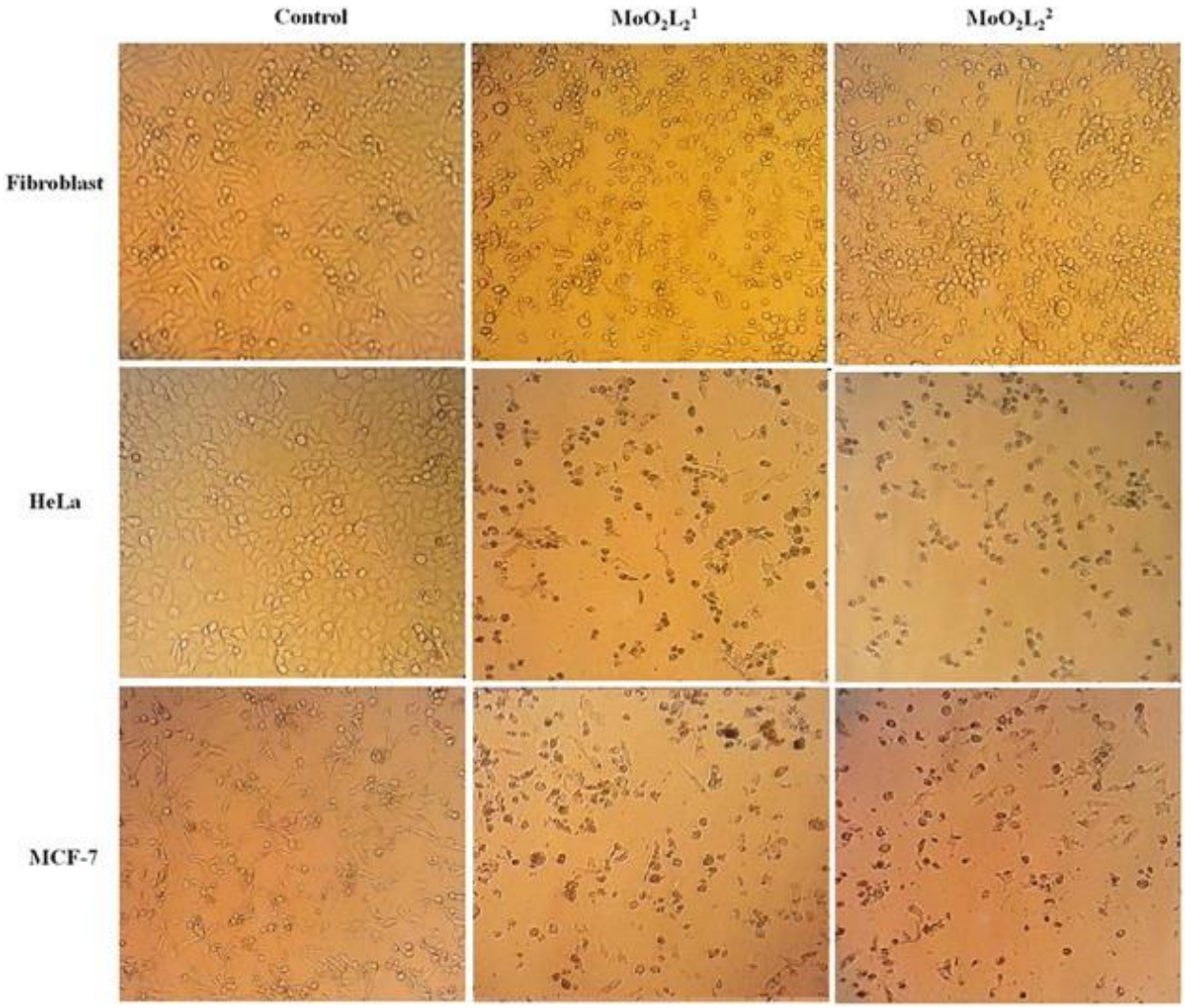

Fig. 16. Morphological changes of normal (fibroblast) and cancer (HeLa and MCF-7) cells after incubation with Mo(VI) complexes for 48 h.

The overall results firmly indicate high potential of these complexes for development of therapeutic agents for cancer therapy. Further investigation regarding to the investigation of the mechanism of anticancer activity of Mo(VI) complexes and also development of targeted delivery systems for their efficient and specific delivery to the related tumors could be suggested toward attaining this goal.

4. Conclusion

This paper reports the synthesis of homochiral (*R,R*/*S,S*) and heterochiral (*R,S*) of a novel dioxomolybdenum complex by using a racemic Schiff base ligand which are diastereomeric pair of Mo complexes [*R,R*/*S,S*-$MoO_2L(LH_2)$ and (*R,S*/*S,R*-$MoO_2L(LH_2)$], named (**$MoO_2L(LH_2)^1$** and **$MoO_2L(LH_2)^2$**). They have been successfully separated using crystallization, and then the structure of homochiral diastereomer was determined by single-crystal X-ray analysis. In addition, this study made a comparison between the anticancer activities of two diastereomers that are not documented in the literatures, in best our knowledge. Their HSA- and DNA-binding study show that there is slight difference between HSA binding affinity with this complexes, while their DNA-binding is considerably difference and **$MoO_2L(LH_2)^2$** exhibited higher binding constant, about 10-fold. Interestingly, the MTT results suggested that the complexes are specific in anticancer activity, **$MoO_2L(LH_2)^1$** exhibits more cytotoxic on MCF-7 cells, but **$MoO_2L(LH_2)^2$** is more potent against HeLa cells.

Acknowledgements

The authors are grateful to the Research Council of the University of Isfahan for financial support of this work.

References

[1] S. Tabassum, A. Asim, R.A. Khan, Z. Hussain, S. Srivastav, S. Srikrishna, F. Arjmand, Chiral heterobimetallic complexes targeting human DNAtopoisomerase Ia, Dalton Trans. 42 (2013) 16749.

[2] M. Benedetti, J. Malina, J. Kasparkova, V. Brabec, G. Natile, Chiral discrimination in platinum anticancer drugs, Environ. Health Perspect. 110 (2002) 779.

[3] X. Zhang, Z.-X. Lei, W. Luo, W.-Q. Mu, X. Zhang, Q.-Y. Zhu, J. Dai, 1-D selenidoindates {[In2Se5]}1 directed by chiral metal complex cations of 1,10-phenanthroline, Inorg. Chem. 50 (2011) 10872.

[4] M. Li, S.E. Howson, K. Dong, N. Gao, J. Ren, P. Scott, X. Qu, Chiral metallohelical complexes enantioselectively target amyloid b for treating Alzheimer's disease, J. Am. Chem. Soc. 136 (2014) 11655.

[5] B.-L. Fei, W.-S. Xu, H.-W. Tao, W. Li, Y. Zhang, J.-Y. Long, Q.-B. Liu, B. Xia, W.-Y. Sun, Effects of copper ions on DNA binding and cytotoxic activity of a chiral salicylidene Schiff base, J. Photochem. Photobiol., B 132 (2014) 36.
[6] R. Alizadeh, M. Afzal, F. Arjmand, In vitro DNA binding, pBR322 plasmid cleavage and molecular modeling study of chiral benzothiazole Schiff-basevaline Cu (II) and Zn (II) complexes to evaluate their enantiomeric biological disposition for molecular target DNA, Spectrochim. Acta A 131 (2014) 625.
[7] N.-U.H. Khan, N. Pandya, K.J. Prathap, R.I. Kureshy, S.H.R. Abdi, S. Mishra, H.C. Bajaj, Chiral discrimination asserted by enantiomers of Ni (II), Cu (II) and Zn (II) Schiff base complexes in DNA binding, antioxidant and antibacterial activities, Spectrochim. Acta A 81 (2011) 199.
[8] F. Arjmand, F. Sayeed, M. Muddassir, Synthesis of new chiral heterocyclic Schiff base modulated Cu (II)/Zn (II) complexes: their comparative binding studies with CT-DNA, mononucleotides and cleavage activity, J. Photochem. Photobiol., B 103 (2011) 166.
[9] M. Khorshidifard, H.A. Rudbari, Z. Kazemi-Delikani, V. Mirkhani, R. Azadbakht, Synthesis, characterization and X-ray crystal structures of vanadium (IV), cobalt (III), copper (II) and zinc (II) complexes derived from an asymmetric bidentate Schiff-base ligand at ambient temperature, J. Mol. Struct. 1081 (2015) 494.
[10] M. Khorshidifard, H.A. Rudbari, B. Askari, M. Sahihi, M.R. Farsani, F. Jalilian, G. Bruno, Cobalt (II), copper (II), zinc (II) and palladium (II) Schiff base complexes: synthesis, characterization and catalytic performance in selective oxidation of sulfides using hydrogen peroxide under solvent-free conditions, Polyhedron 95 (2015) 1.
[11] Z. Kazemi, H.A. Rudbari, V. Mirkhani, M. Sahihi, M. Moghadam, S. Tangestaninejad, I. Mohammadpoor-Baltork, Synthesis, characterization, crystal structure, DNA-and HSA-binding studies of a dinuclear Schiff base Zn (II) complex derived from 2-hydroxynaphtaldehyde and 2-picolylamine, J. Mol. Struct. 1096 (2015) 110.
[12] Z. Kazemi, H.A. Rudbari, M. Sahihi, V. Mirkhani, M. Moghadam, S.

Tangestaninejad, I. Mohammadpoor-Baltork, S. Gharaghani, Synthesis, characterization and biological application of four novel metal-Schiff base complexes derived from allylamine and their interactions with human serum albumin: experimental, molecular docking and ONIOM computational study, J. Photochem. Photobiol., B 162 (2016) 448.
[13] Z. Kazemi, H. Amiri Rudbari, V. Mirkhani, M. Sahihi, M. Moghadam, S. Tangestaninejad, I. Mohammadpoor-Baltork, A. Abbasi Kajani, G. Azimi, Selfrecognition of the racemic ligand in the formation of homochiral dinuclear V (V) complex: in vitro anticancer activity, DNA and HSA interaction, Eur. J. Med. Chem. 135 (2017) 230.
[14] P. Bagi, T. Kovács, T. Szilvási, P. Pongrácz, L. Kollár, L. Drahos, E. Fogassy, G. Keglevich, Platinum (II) complexes incorporating racemic and optically active 1-alkyl-3-phospholene P-ligands: synthesis, stereostructure, NMR properties and catalytic activity, J. Organomet. Chem. 751 (2014) 306.
[15] A. Woo, Y.H. Lee, S. Hayami, L.F. Lindoy, P. Thuéry, Y. Kim, Comparative investigation of the copper (II) complexes of (R)-,(S)-and (R, S)-1-phenyl-N, Nbis (pyridine-3-ylmethyl) ethanamine along with the related complex of (R, S)-1-cyclohexyl-N, N-bis (pyridine-3-ylmethyl) ethanamine. Synthetic, magnetic, and structural studies, J. Incl. Phenom. Macrocycl. Chem. 71 (2011) 409.
[16] H. Brunner, M. Niemetz, M. Zabel, Optisch aktive Übergangsmetall-Komplexe, 122. Synthese von Palladium (II)-Schiff-base-komplexen-intramolekulare wechselwirkungen/optically active transition metal complexes, 122. Synthesis of palladium (II) complexes with Schiff base ligandsintramolecular interactions, Z. Naturforsch., B 55 (2000) 145.
[17] S. Cie, Program for the Acquisition and Analysis of Data XeAREA, version1. 30, Stoe & Cie GmbH, Darmatadt, Germany, 2005.
[18] C. Stoe, X-SHAPE, Version 2.05, Program for Crystal Optimization for Numerical Absorption Correction, Stoe & Cie GmbH, Darmatadt, Germany, 2004.
[19] M.C. Burla, R. Caliandro, M. Camalli, B. Carrozzini, G.L. Cascarano, L. De Caro, C.

Giacovazzo, G. Polidori, R. Spagna, SIR2004: an improved tool for crystal structure determination and refinement, J. Appl. Crystallogr. 38 (2005) 381.
[20] K. Zheng, F. Liu, X.-M. Xu, Y.-T. Li, Z.-Y. Wu, C.-W. Yan, Synthesis, structure and molecular docking studies of dicopper (II) complexes bridged by N-phenolato-N0-[2-(dimethylamino) ethyl] oxamide: the influence of terminal ligands on cytotoxicity and reactivity towards DNA and protein BSA, New J. Chem. 38 (2014) 2964.
[21] B. Guhathakurta, P. Basu, C.S. Purohit, N. Bandyopadhyay, G.S. Kumar, S. Chowdhury, J.P. Naskar, Synthesis, characterization, structure, DNA binding aspects and molecular docking study of a novel Schiff base ligand and its bis (l-chloro) bridged Cu (II) dimer, Polyhedron 126 (2017) 195.
[22] H.V.R. Silva, J.S.M. Dias, G.Á. Ferreira-Silva, L.C. Vegas, M. Ionta, C.C. Corrêa, A.A. Batista, M.I.F. Barbosa, A.C. Doriguetto, Phosphine/diimine ruthenium complexes with Cl_, CO, NO+, NO2_, NO3_ and pyridine ligands: proapoptotic activity on triple-negative breast cancer cells and DNA/HSA interactions, Polyhedron 144 (2018) 55.
[23] M.J. Frisch, G.W. Trucks, H.B. Schlegel, G.E. Scuseria, J.R.C.M.A. Robb, G. Scalmani, V. Barone, G.A.P.B. Mennucci, H. Nakatsuji, M. Caricato, H.P.H.X. Li, A. F. Izmaylov, J. Bloino, G. Zheng, M.H.J.L. Sonnenberg, M. Ehara, K. Toyota, J.H.R. Fukuda, M. Ishida, T. Nakajima, Y. Honda, H.N.O. Kitao, T. Vreven, J.A. Montgomery Jr, F.O.J.E. Peralta, M. Bearpark, J.J. Heyd, K.N.K.E. Brothers, V.N. Staroverov, R. Kobayashi, K.R.J. Normand, A. Rendell, J.C. Burant, J.T.S.S. Iyengar, M. Cossi, N. Rega, J.M. Millam, J.E.K.M. Klene, J.B. Cross, V. Bakken, C. Adamo, R.G.J. Jaramillo, R.E. Stratmann, O. Yazyev, R.C.A.J. Austin, C. Pomelli, J.W. Ochterski, K.M.R.L. Martin, V.G. Zakrzewski, G.A. Voth, J.J.D.P. Salvador, S. Dapprich, A.D. Daniels, J.B.F.O. Farkas, J.V. Ortiz, J. Cioslowski, D.J. Fox, Gaussian Development Version Revision B.01, Gaussian. Inc., Wallingford CT, 2009.
[24] G.M. Morris, D.S. Goodsell, R.S. Halliday, R. Huey, W.E. Hart, R.K. Belew, A.J. Olson, Automated docking using a Lamarckian genetic algorithm and an empirical binding free energy function, J. Comput. Chem. 19 (1998) 1639.
[25] J.D. Chellaian, J. Johnson, Spectral characterization, electrochemical and

anticancer studies on some metal (II) complexes containing tridentate quinoxaline Schiff base, Spectrochim. Acta, Part A 127 (2014) 396.
[26] A.A. Kajani, A.-K. Bordbar, S.H.Z. Esfahani, A. Razmjou, Gold nanoparticles as potent anticancer agent: green synthesis, characterization, and in vitro study, RSC Adv. 6 (2016) 63973.
[27] M. Dey, C.P. Rao, P.K. Saarenketo, K. Rissanen, E. Kolehmainen, P. Guionneau, Mn (IV) and Co (III)-complexes of –OH-rich ligands possessing O2N, O3N and O4N cores: syntheses, characterization and crystal structures, Polyhedron 22 (2003) 3515.
[28] H.A. Rudbari, M. Khorshidifard, B. Askari, N. Habibi, G. Bruno, New asymmetric Schiff base ligand derived from allylamine and 2,3-dihydroxybenzaldehyde and its molybdenum (VI) complex: synthesis, characterization, crystal structures, computational studies and antibacterial activity together with synergistic effect against Pseudomonas aeroginosa PTTC 1570, Polyhedron 100 (2015) 180.
[29] J. Feng, X.-M. Lu, G. Wang, S.-Z. Du, Y.-F. Cheng, The syntheses and characterizations of molybdenum (vi) complexes with catechol and 2,3-dihydroxynaphthalene, and the structure–effect relationship in their in vitro anticancer activities, Dalton Trans. 41 (2012) 8697.
[30] M. Enamullah, A.R. Uddin, G. Pescitelli, R. Berardozzi, G. Makhloufi, V. Vasylyeva, A.-C. Chamayou, C. Janiak, Induced chirality-at-metal and diastereoselectivity at D/K-configured distorted square-planar copper complexes by enantiopure Schiff base ligands: combined circular dichroism, DFT and X-ray structural studies, Dalton Trans. 43 (2014) 3313.
[31] A.-C. Chamayou, S. Lüdeke, V. Brecht, T.B. Freedman, L.A. Nafie, C. Janiak, Chirality and diastereoselection of D/K-configured tetrahedral zinc complexes through enantiopure Schiff base complexes: combined vibrational circular dichroism, density functional theory, 1H NMR, and X-ray structural studies, Inorg. Chem. 50 (2011) 11363.
[32] S. Rayati, N. Rafiee, A. Wojtczak, cis-Dioxo-molybdenum (VI) Schiff base complexes: synthesis, crystal structure and catalytic performance for

homogeneous oxidation of olefins, Inorg. Chim. Acta 386 (2012) 27.
[33] M.E. Judmaier, C. Holzer, M. Volpe, N.C. Mösch-Zanetti, Molybdenum (VI) dioxo complexes employing Schiff base ligands with an intramolecular donor for highly selective olefin epoxidation, Inorg. Chem. 51 (2012) 9956.
[34] N. Tadayonpour, S. Rayati, M.H. Sadr, K. Zare, A. Wojtczak, A cisdioxomolybdenum Schiff base complex: synthesis, crystal structure and catalytic activity in oxidation of olefins using hydrogen peroxide, Transit. Met. Chem. 40 (2015) 891.
[35] S.S. Paul, M. Selim, A. Saha, K.K. Mukherjea, Synthesis and structural characterization of dioxomolybdenum and dioxotungsten hydroxamato complexes and their function in the protection of radiation induced DNA damage, Dalton Trans. 43 (2014) 2835.
[36] J.-P. Cao, L.-L. Zhou, L.-Z. Fu, J.-X. Zhao, H.-X. Lu, S.-Z. Zhan, A molybdenum–Schiff base complex, a new molecular electro-catalyst for generating hydrogen from acetic acid or water, Catal. Commun. 57 (2014) 1.
[37] Z. Kazemi, H.A. Rudbari, M. Sahihi, V. Mirkhani, M. Moghadam, S. Tangestaninejad, I. Mohammadpoor-Baltork, G. Azimi, S. Gharaghani, A.A. Kajani, Synthesis, characterization and separation of chiral and achiral diastereomers of Schiff base Pd (II) complex: a comparative study of their DNA-and HSA-binding, J. Photochem. Photobiol., B 163 (2016) 246.
[38] M. Cindric´ , N. Strukan, V. Vrdoljak, T. Kajfezˇ, B. Kamenar, A series of molybdenum (VI) complexes with tridentate Schiff base ligands, Z. Anorg. Allg. Chem. 628 (2002) 2113.
[39] M. Niaz, S. Iran, R. Abdolreza, Methanoldioxido {1-[(2RS)-(2-oxidopropyl) iminomethyl]-2-naphtholato} molybdenium VI, Acta Crystallogr. Sect. E: Struct. Rep. Online 66 (2010), m202-m202.
[40] I. Sheikhshoaie, A. Rezaeifard, N. Monadi, S. Kaafi, A novel tridentate Schiff base dioxo-molybdenum (VI) complex: synthesis, crystal structure and catalytic performance in green oxidation of sulfides by urea hydrogen peroxide, Polyhedron 28 (2009) 733.
[41] C. Zhang, G. Rheinwald, V. Lozan, B. Wu, P.G. Lassahn, H. Lang, C. Janiak,

Structural study and solution integrity of dioxomolybdenum (VI) complexes with tridentate Schiff base and azole ligands, Z. Anorg. Allg. Chem. 628 (2002)
1259.
[42] Y. Sui, X. Zeng, X. Fang, X. Fu, Y.A. Xiao, L. Chen, M. Li, S. Cheng, Syntheses, structure, redox and catalytic epoxidation properties of dioxomolybdenum (VI) complexes with Schiff base ligands derived from tris (hydroxymethyl) amino methane, J. Mol. Catal. A: Chem. 270 (2007) 61.
[43] J. Liimatainen, A. Lehtonen, R. Sillanpää, cis-Dioxomolybdenum (VI) complexes with tridentate and tetradentate Schiff base ligands, Preparation, structures and inhibition of aerial oxidation of aldehydes, Polyhedron 19 (2000) 1133.
[44] D. Agustin, J.-C. Daran, R. Poli, Polymorph of 2-[(2-hydroxyethyl) iminiomethyl] phenolato-jO dioxido 2-[(2-oxidoethyl) iminomethyl] phenolato-j3O, N, O0 molybdenum (VI), Acta Crystallogr., Sect. C: Cryst. Struct. Commun. 64 (2008) m101.
[45] T. Głowiak, L. Jerzykiewicz, J.M. Sobczak, J.J. Ziółkowski, New insights into the chemistry of oxomolybdenum (VI) complexes with N-salicylidene-2-aminoethanol, Inorg. Chim. Acta 356 (2003) 387.
[46] C.V. Garcia, G.L. Parrilha, B.L. Rodrigues, S.F. Teixeira, R.A. de Azevedo, A.K. Ferreira, H. Beraldo, Tricarbonylrhenium (I) complexes with 2-acetylpyridinederived hydrazones are cytotoxic to NCI-H460 human large cell lung cancer, New J. Chem. 40 (2016) 7379.
[47] W. Li, Y. Ding, X.-S. Cheng, Z. You, Synthesis, crystal structures and preliminary antibacterial activities of nickel (II) and zinc (II) complexes derived from 2-bromo-6-[(3-cyclohexylaminopropylimino) methyl] phenol, J. Chil. Chem. Soc. 60 (2015) 3034.
[48] P. Chakraborty, I. Majumder, K.S. Banu, B. Ghosh, H. Kara, E. Zangrando, D. Das, Mn (II) complexes of different nuclearity: synthesis, characterization and catecholase-like activity, Dalton Trans. 45 (2016) 742.
[49] T. Steiner, The hydrogen bond in the solid state, Angew. Chem. Int. Ed. 41 (2002) 48.
[50] P. Kalaivani, R. Prabhakaran, F. Dallemer, P. Poornima, E. Vaishnavi, E.

Ramachandran, V.V. Padma, R. Renganathan, K. Natarajan, DNA, protein binding, cytotoxicity, cellular uptake and antibacterial activities of new palladium (II) complexes of thiosemicarbazone ligands: effects of substitution on biological activity, Metallomics 4 (2012) 101.
[51] M. Kalita, K.J. Tamuli, P. Barman, B. Sarma, R. Baruah, H.P.D. Boruah, Synthesis, crystal structure, bioactivities of Ni (II), Cu (II), Co (II) and Pd (II) complexes with unsymmetrical thioether donor Schiff base: phosphine free Pd (II) complex catalyzed Suzuki reaction, Polyhedron 97 (2015) 140.
[52] S.S. Bhat, A.A. Kumbhar, H. Heptullah, A.A. Khan, V.V. Gobre, S.P. Gejji, V.G. Puranik, Synthesis, electronic structure, DNA and protein binding, DNA cleavage, and anticancer activity of fluorophore-labeled copper (II) complexes, Inorg. Chem. 50 (2010) 545.
[53] P. Vasantha, B. Sathish, Kumar, B. Shekhar, P. Anantha Lakshmi, Cobalt (II)–metformin complexes containing a-diimine/a-diamine as auxiliary ligand: DNA binding properties, Appl. Organomet. Chem. 32 (2018) e4074.
[54] A.S. Abu-Surrah, H.H. Al-Sa'doni, M.Y. Abdalla, Palladium-based chemotherapeutic agents: routes toward complexes with good antitumor activity, Cancer therapy 6 (2008) 1.
[55] E.M. Mrkalic´ , R.M. Jelic´ , O.R. Klisuric´ , Z.D. Matovic´ , Synthesis of novel palladium (II) complexes with oxalic acid diamide derivatives and their interaction with nucleosides and proteins. Structural, solution, and computational study, Dalton Trans. 43 (2014) 15126.
[56] S.U. Dighe, S. Khan, I. Soni, P. Jain, S. Shukla, R. Yadav, P. Sen, S.M. Meeran, S. Batra, Synthesis of b-carboline-based N-heterocyclic carbenes and their antiproliferative and anti-metastatic activities against human breast cancer cells, J. Med. Chem. 58 (8) (2015) 3485.
[57] P. Lincoln, E. Tuite, B. Nordén, Short-circuiting the molecular wire: cooperative binding of D-[Ru (phen) 2d ppz] 2+ and D-[Rh (phi) 2bipy] 3+ to DNA, J. Am. Chem. Soc. 119 (1997) 1454.
[58] X.-L. Li, Y.-J. Hu, H. Wang, B.-Q. Yu, H.-L. Yue, Molecular spectroscopy evidence of berberine binding to DNA: comparative binding and thermodynamic profile

of intercalation, Biomacromolecules 13 (2012) 873.
[59] B. Guhathakurta, P. Basu, G.S. Kumar, L. Lu, M. Zhu, N. Bandyopadhyay, J.P. Naskar, Synthetic, structural, electrochemical and DNA-binding aspects of a novel oximato bridged copper (II) dimer, Polyhedron 110 (2016) 227.
[60] A. Barmpa, O. Frousiou, S. Kalogiannis, F. Perdih, I. Turel, G. Psomas, Manganese (II) complexes of the quinolone family member flumequine: structure, antimicrobial activity and affinity for albumins and calf-thymus DNA, Polyhedron 145 (2018) 166.
[61] D. Varna, E. Kapetanaki, A. Koutsari, A.G. Hatzidimitriou, G. Psomas, P. Angaridis, R. Papi, A.A. Pantazaki, P. Aslanidis, Heterocyclic thioamide/ phosphine mixed-ligand silver (I) complexes: synthesis, molecular structures, DNA-binding properties and antibacterial activity, Polyhedron (2018).
[62] F.J. Fard, Z.M. Khoshkhoo, H. Mirtabatabaei, M. Housaindokht, R. Jalal, H.E. Hosseini, M. Bozorgmehr, A. Esmaeili, M.J. Khoshkholgh, Synthesis, characterization and interaction of N,N0-dipyridoxyl (1,4-butanediamine) Co (III) salen complex with DNA and HSA, Spectrochim. Acta A 97 (2012) 74.
[63] A. Das, G.S. Kumar, Binding studies of aristololactam-b-d-glucoside and daunomycin to human serum albumin, RSC Adv. 4 (2014) 33082.
[64] H.K. Noor-ul, N. Pandya, N.C. Maity, M. Kumar, R.M. Patel, R.I. Kureshy, S.H. Abdi, S. Mishra, S. Das, H.C. Bajaj, Influence of chirality of V (V) Schiff base complexes on DNA, BSA binding and cleavage activity, Eur. J. Med. Chem. 46 (2011) 5074.
[65] N. Fani, A. Bordbar, Y. Ghayeb, A combined spectroscopic, docking and molecular dynamics simulation approach to probing binding of a Schiff base complex to human serum albumin, Spectrochim. Acta Mol. Biomol. Spectrosc. 103 (2013) 11.
[66] F. Deng, Y. Liu, Study of the interaction between tosufloxacin tosylate and bovine serum albumin by multi-spectroscopic methods, J. Lumin. 132 (2012) 443.
[67] X.-B. Fu, G.-T. Weng, D.-D. Liu, X.-Y. Le, Synthesis, characterization, DNA,

binding and cleavage, HSA interaction and cytotoxicity of a new copper (II) complex derived from 2-(20-pyridyl) benzothiazole and glycylglycine, J. Photochem. Photobiol., A 276 (2014) 83.
[68] J. Ghuman, P.A. Zunszain, I. Petitpas, A.A. Bhattacharya, M. Otagiri, S. Curry, Structural basis of the drug-binding specificity of human serum albumin, J. Mol. Biol. 353 (2005) 38.
[69] I. Agranat, H. Caner, J. Caldwell, Putting chirality to work: the strategy of chiral switches, Nat. Rev. Drug Discov. 1 (2002) 753.